Specialty Wood Products Research Partnership

UC UNIVERSITY OF CANTERBURY
Te Whare Wānanga o Waitaha
CHRISTCHURCH NEW ZEALAND

Theme: Specialty Wood Products (SWP)

PROJECT REPORT

Work Plan No. SWP-WP065

Milestone Number: 1.2.6.3

Experimental studies on Douglas-fir CLT connections and core-walls

Authors:

Minghao Li

Justin Brown

Research Provider:
UC

Date: 28 June19
Rev. A SWP-T082

EXECUTIVE SUMMARY

This project report summarizes the experimental testing results of Douglas-fir Cross-laminated Timber (CLT) connections and core-walls. 54 screwed connection tests were performed under both monotonic and cyclic loading, and 31 castellated connection tests were performed under monotonic loading. A total of 18 tests were performed in the core-wall system testing phase. It was found that mixed angle screwed connections showed significant displacement capacity, high strength and stiffness and are suitable for seismic design of CLT buildings with moderate or high ductility in New Zealand. Castellated connections showed high strength capacity and are an efficient connection type for transferring shear loads between CLT panels. The core-wall testing results showed that significant increases in strength and stiffness are achievable when considering the contribution from orthogonal walls. Meanwhile, it was found that mixed angle screwed connections were able to increase the robustness of the connections between CLT wall panels, thus increasing the coupling effect or composition action in the core-walls as well as energy dissipation of the core-wall system. The experimental testing results provided strong technical evidence that the CLT core-walls can provide more efficient lateral load resisting systems for mid-rise and high-rise timber buildings.

TABLE OF CONTENTS

1 INTRODUCTION

Emerging timber technologies, environmental awareness, increased urbanization, and the architectural desire for exposed timber members have led to increased interest in engineered timber construction. Timber is experiencing a renaissance as a building material, supported by innovative fabrication and construction technologies which produce engineered wood products (EWPs) to a high level of prefabrication and allow for efficient and safe installation. New construction with EWPs including Cross-laminated timber (CLT) around the world confirms that timber buildings can provide a cost-effective, timely solution when chosen for a suitable building occupancy. So far CLT production in New Zealand (NZ) is dominated by Radiata pine and research on the structural performance of CLT is focused on Radiata pine. However, there is a significant resource of Douglas-fir available in NZ, which is currently not widely processed on-shore. CLT is a potential high-value building product for the NZ Douglas-fir resource but the design properties of Douglas-fir CLT and the associated connection behaviour remain largely unknown. The lack of enough knowledge may hinder the use of Douglas-fir in CLT construction. Thus, there is a need to establish a comprehensive database of the mechanical properties of Douglas-fir CLT and the common connection systems so that design engineers will be able to specify Douglas-fir CLT in timber building design.

This project is an extension of previous work on Douglas-fir CLT at UC to understand commonly used CLT connections with the capstone testing on an innovative structural CLT core-wall system. The objective of the connection testing is to establish an experimental database to understand the behaviour of screwed and castellated Douglas-fir CLT connections that are also commonly used in CLT building construction. In particular, the connections with long self-tapping screws (STS) are widely used in CLT residential buildings to connect floors and walls. This is shown in Figure 1. Limited knowledge is available on the behaviour of these types of connections under seismic loading since most of previous CLT connection research is not focused on seismic behaviour. For timber buildings built in high seismic countries like NZ, connection design is critical because connections are the main source of ductility and dissipating energy for timber buildings. For the castellated connections, as shown in Figure 2, monotonic loading will be applied because these connections are designed to transfer shear loads and not considered as an energy dissipating source for CLT buildings. Therefore, only strength and stiffness properties are evaluated.

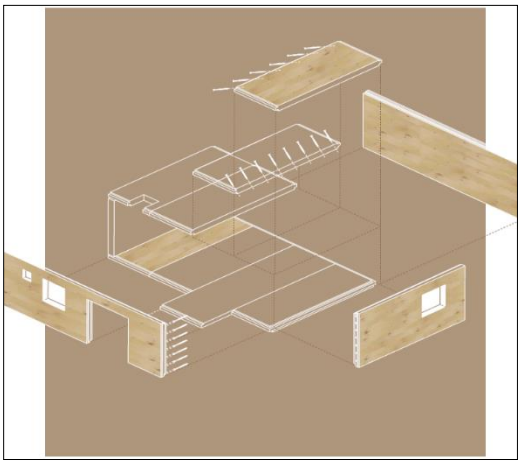

Figure 1: Screwed connections in CLT (Green & Taggart, 2017)

Figure 2: Castellated connection in NZ CLT Building (c/o Sam Leslie)

The in-plane behaviour of typical CLT walls are well experimentally tested and researched. Very limited knowledge is available to quantify the contribution of returning walls under seismic loading. Orthogonal walls in CLT buildings are often connected with STS, but this is primarily done for constructability as the added benefit of these walls is not known. The first portion of this project will assess the performance of STS connections in CLT, and the core-wall testing phase will assess the core-wall behaviour by implementing the STS connections at the system level. For timber buildings built in high seismic countries like NZ, seismic force demand is large and the core-wall systems with reliable composition between orthogonal walls will increase lateral strength and stiffness of CLT buildings and improve the structural efficiency. In particular, commercial buildings with open concept floor plans have limited length of walls to be designed as two-dimensional walls. Thus, the formation of core-wall systems with enough composite action can offer a robust solution of lateral force resisting systems for these buildings. In this project, critical properties of the CLT core-wall systems such as strength, stiffness will be evaluated. Figure 3 shows a recently completed hybrid CLT concrete core project. The objective of the core-wall testing phase is to experimentally test and quantify how efficient a CLT core-wall structure could be to resist seismic forces.

Figure 3: Hybrid CLT building with concrete core (Seagate Structures, n/a)

1.1 Description of CLT Specimens

The CLT specimens are made of lamstock provided by Sutherland Timber Co.. The Douglas-fir lamstock was sourced from Hamner Springs with the grade SG8. The CLT specimens were manufactured by XLam Ltd. with the following lay-ups and thicknesses in Table 1. Table 2 outlines

the lamination widths and depths. The screwed and castellated connection tests were performed using both CLT5 and CLT7 panels while core-wall testing used CLT5.

Table 1: CLT Specimens

CLT Type	*Total Thickness (mm)*	*Lay-ups (mm)*
CLT5 (5-Ply)	175	45/20/45/20/45
CLT7 (7-Ply)	275	45/35/35/45/35/35/45

Table 2: CLT Lamstock Properties

Layer Thickness (mm)	*Board Width (mm)*	*Board Thickness (mm)*
20	150+	25
35	200+	40
45	200+	50

In the production process, deficiencies in timber boards such as knots and slope of grain were removed and the boards are then finger-jointed by a mechanical press to lengths up to 15m. The jointed pieces were planed to laminations with precise dimensions of, for example, 20mmx150mm. The CLT panels were pressed in a vacuum press with Purbond one-component polyurethane glue, which can produce panels of a maximum size of 15m x 3.4m. The CLT specimens were face bonded only to each adjacent board without edge-gluing. The gaps between adjacent laminations can help relieve the stresses due to differential shrinkage or swelling and facilitate the pressing process. Figure 4 shows a typical 5-ply CLT panel for reference.

Figure 4: An example of Cross-laminated Timber (CLT)

2 DESCRIPTION OF TEST PROGRAMME

The test programme consists of screwed and castellated connection testing and large scale CLT core-wall testing. Connection testing were carried out in the Structural Wing Lab while core-wall testing were performed in the Structural Engineering Laboratory (SEL) at the University of Canterbury.

2.1 Screwed Connection Testing

A total of 54 screwed connection tests were performed under both monotonic and cyclic loading. Spax screws were fully threaded with equal penetration depth on each timber member. ø8mm and ø12mm screws were used for CLT5 and CLT7 testing respectively. Figures 5 and 6 show the test schematics of the screwed connections with inclined screws to connect two side members and one middle member. Figure 7 shows the schematic of screws installed with mixed angles (inclined and 90-degrees).

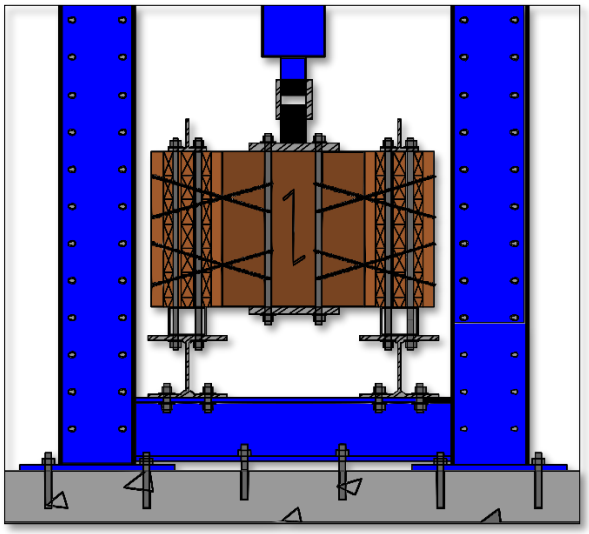

Figure 5: Test schematic

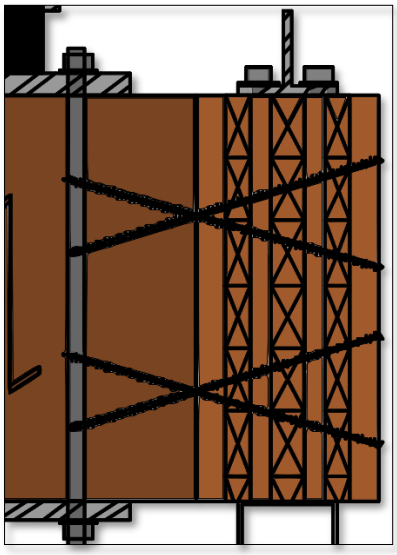

Figure 6: Inclined screw detail

Figure 7: CLT7 mixed screw test

Figure 8 shows a photo of the test set-up of the screwed connections in the lab. A 1000kN actuator was clamped to the middle CLT panel while the outer two panels were restrained from both vertical and lateral movement. This set-up enabled the actuator to push and pull the middle panel to replicate cyclic loading. Table 3 below lists the test matrix describing the screwed connection testing programme.

Figure 8: Screwed connection testing set-up

Table 3: Screwed connection testing matrix

	CLT 5					*CLT7*		
Screw Dia. (mm)			8				12	
Series	400X	200X	16X+16	8T	8C	375X	12X+4	12X+6
Inclined Screws (screw length)	16 (400)	16 (200)	16 (200)	8 (200)	8 (200)	12 (375)	12 (375)	12 (375)
90 Deg. (screw length)	0	0	16 (350)	0	0	0	4 (550)	6 (550)
Ratio	n/a	n/a	1:1	n/a	n/a	n/a	3:1	2:1
Monotonic Tests	3	3	3	3	3	3	3	3
Cyclic Tests	5	5	5			5	5	5

Note:
400X – Screw length and in cross configuration
8T / 8C – 8 tension or compression screws
Ratio - between the number of inclined screws and the number of 90 degree installed screws

Monotonic tests were performed following EN 26891 (1991), as shown in Figure 9. The yield displacement was calculated following EN12512, shown in Figure 10, with the average monotonic curve used for the input parameters to determine the cyclic loading protocol. All cyclic tests were performed following the loading protocol described in EN12512 (2005), shown in Figure 11.

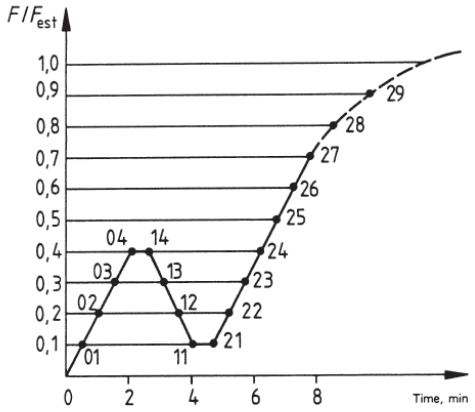

Figure 1 — Loading procedure

Figure 9: EN26891 monotonic loading protocol

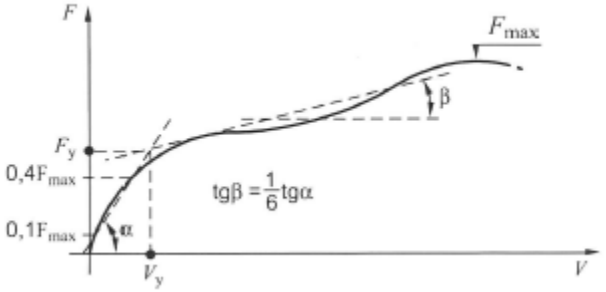

Figure 10: EN12512 yield displacement determination

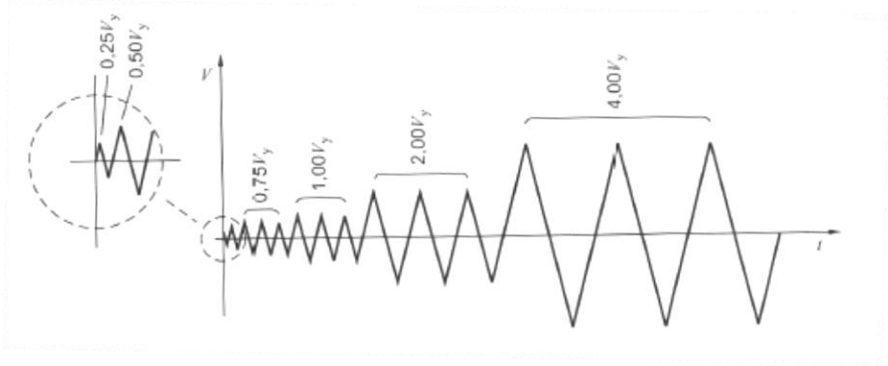

Figure 11: EN12512 cyclic loading protocol

2.2 Castellated Connection Testing

A total of 31 castellated connection tests were performed under monotonic loading as this type of connection is not designed as a ductile connection in CLT buildings. Both CLT5 and CLT7 panels were used to fabricate the connections, and the test set-up schematic and the aspect ratio of the notches are shown in Figure 12 and Figure 13.

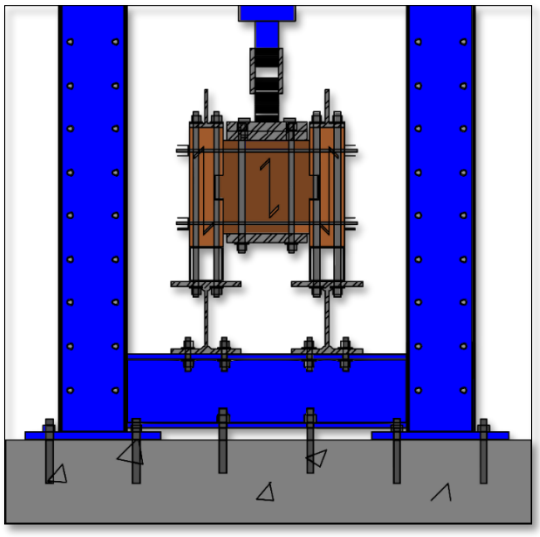

Figure 12: Castellated testing schematic

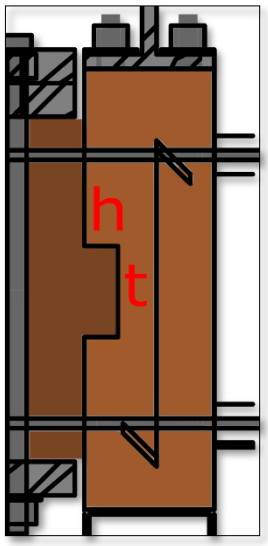

Figure 13: Aspect ratio detail

The aspect ratio h/t was varied in the test specimens to study different failure mechanisms based on predictions. The experimental test set-up photo is shown in Figure 14. Three CLT panels were connected with the castellation, and the middle specimen was pushed down with the 1000kN actuator via a loading plate. The panels were restrained from horizontal movement, and the relative vertical movement between the middle and outer panels both inside and outside the castellation were recorded.

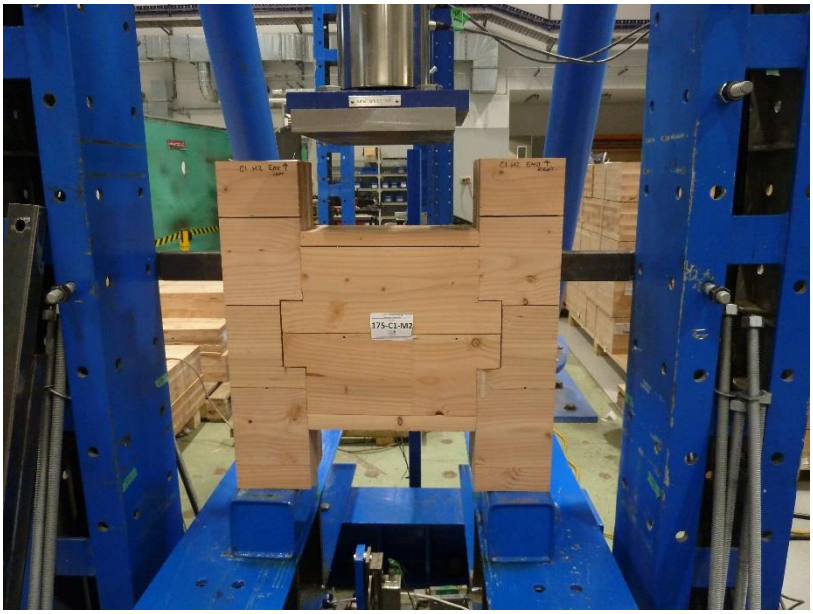

Figure 14: Castellated connection test set-up

Table 4 below lists the test matrix describing the castellated connection testing programme.

Table 4: Castellated connection testing matrix

	Perpendicular to Grain		*Parallel to Grain*	
	C1	C2	C3	C4
t:h ratio (mm)	150:50	100:50	105:35	75:100
Possible Failure Mode	Shear	Shear	Shear	Bending
CLT5 Tests	4	3 + 1	3 + 1	3 + 1
CLT7 Tests	3 + 1	3 + 1	3	3 + 1

Note:
+ 1 – Indicated that an additional test was performed where the castellation was reinforced with fully threaded screws.

All monotonic tests were performed following EN 26891 (1991).

2.3 Core-wall System Testing

The lateral behaviour of a 2/3 scale, 8.6m high post-tensioned and conventional CLT core-walls were examined. The main objective was to understand the influence of wall connections on composite action of the core-wall system. CLT5 was used in this test phase with ø26.5mm unbonded post-tensioned steel tendons. A total of 18 tests were performed in the testing programme. In order to adequately decouple the system for subsequent detailed analysis, the test programme was split in three phases: (I) single wall testing, (II) coupled wall testing, and (III) core-wall testing, as shown in Figure 15. Figure 16 shows the predicted wall response at the three test phases, showing the significant difference of strength and stiffness between them.

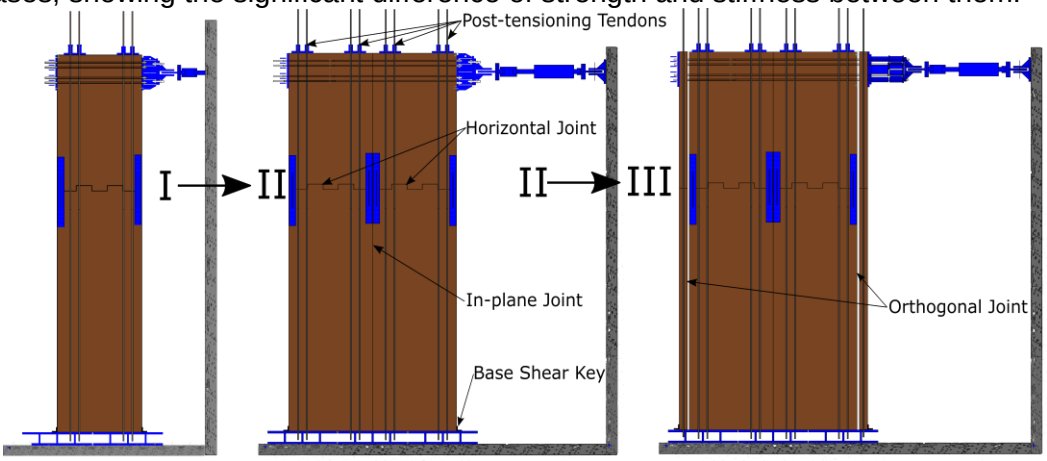

Figure 15: CLT core-wall testing phases

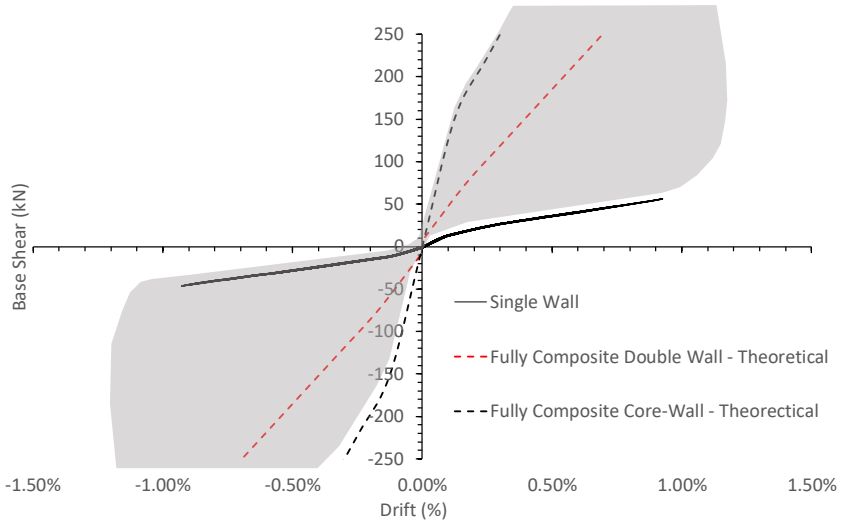

Figure 16: Composite action potential of CLT core-wall system

Phases I and II were tested as post-tensioned CLT rocking walls, and Phase III included both a post-tensioned CLT rocking core-wall and conventional core-wall system. Test matrices of different test phases are shown in Table 5, Table 6, and Table 7, respectively.

Table 5: Phase I single wall test matrix

Test	*1*	*2*	*3*	*4*	*5*
Initial PT level / bar (total initial PT force)	0 kN	25 kN (100kN)	50 kN (200 kN)	75 kN (300kN)	25kN (100kN), two rocking interfaces

Table 6: Phase II coupled wall test matrix

Test	*1*	*2*	*3*	*4*	*5*
In-plane Connection	Friction	8x80 @ 400 O.C. 17mm ply. 90 degree installation angle	8x80 @ 100 O.C. 17mm ply. 90 degree installation angle	8x80 @ 400 O.C. 17mm ply. 90 degree installation angle	Friction
UFP base of each wall	No	No	No	Yes	Yes

Table 7: Phase III core-wall test matrix

	Test 1	*Test 2*	*Test 3*	*Test 4*	*Test 5*	*Test 6*	*Test 7*	*Test 8*
Loading Protocol	1	1	1	2	1	1	2	1
Orthogonal Joint	Fric.	8x350 @ 80mm O.C.	Frict.	Frict.	8x220 @ 30 deg. +15 deg. @ 80mm O.C. in "X" pattern	8x200@ 30 deg. +15 deg. @ 160mm O.C. in "X" pattern + 8x350mm at 90 deg. @ 80mm O.C.	8x350 @ 80mm O.C.	Titan TTN240 with LBA 4x60mm nails @ 400mm O.C.
In-plane Joint	Fric.	8x80 @ 50mm O.C. with 17mm ply.	Fric.	Fric.	8x220 @ 45 deg. +45 deg. @ 80mm O.C.	8x160 @ 45 deg. +45 deg. @ 50 mm O.C. + 8x80 @ 90 deg. @ 50 mm O.C. with 22mm ply.	8x80 @ 50mm O.C. with 17mm ply.	8x160. @ 45 deg. +45 deg. @ 100mm O.C. + 8x80 @ 100mm O.C. with 22mm ply.
UFPs at base	No	No	No	No	Yes	Yes	Yes	No
Initial PT force per bar (450kN is yield load)	25kN / bar	75kN / Bar (10% axial load ratio)	75kN / Bar (10% axial load ratio)	75kN / Bar (10% axial load ratio)	75kN / Bar (10% axial load ratio)	75kN / Bar (10% axial load ratio)	25kN / bar	No PT, conventional hold-downs used

Note:
Fric. - Friction
Loading protocol: 1 – uni-directional, 2 – bi-directional cloverleaf

All testing followed the loading protocol outlined in ACI Innovation Task Group 5 (2008), where wall drift magnitude increased by a factor of 1.25. During Phases I and II, wall drifts were limited to less than 1.5% to avoid significant timber crushing at the wall corners and to ensure the specimen was in good condition for Phase III.

In Phases I and II, the specimen was loaded with one 1000kN actuator and out of plane restraint was provided to the CLT walls with two 1000kN actuators per wall located on the other strong wall, as shown in Figure 17 and Figure 18.

Figure 17: Phase I test set-up

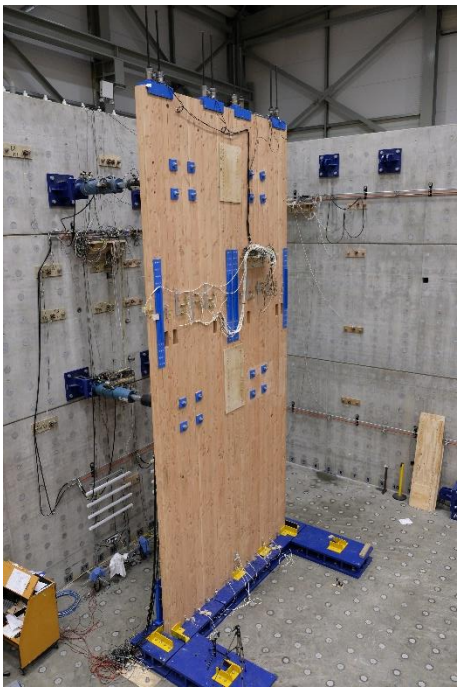

Figure 18: Phase II test set-up

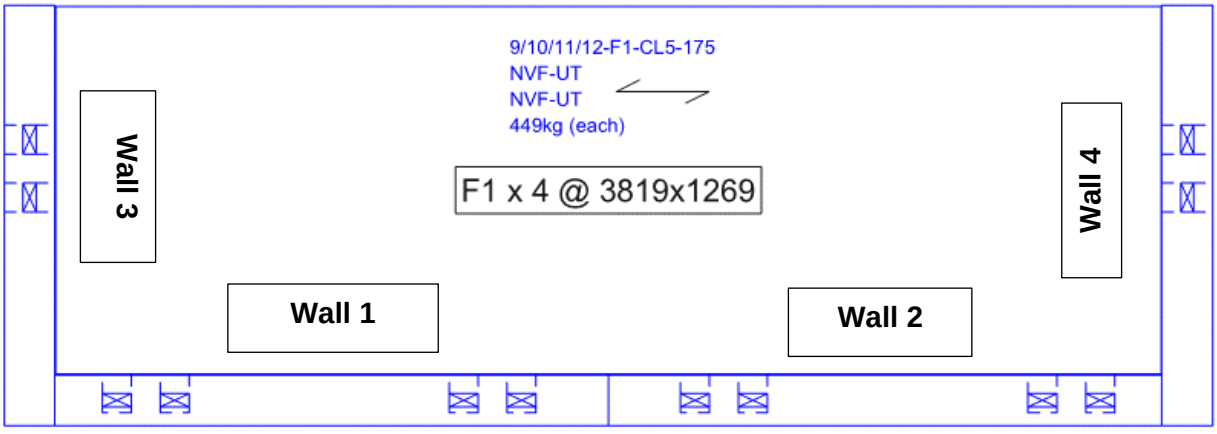

Figure 19: Plan view of core-wall specimen, image from XLam shop drawing

Figure 19 above shows a plan view of the core-wall specimen. For Phase I, only Wall 1 was tested. For Phase II, Walls 1 and 2 were tested together, and for Phase III Walls 3 and 4 were added with CLT floors to create a “C” shaped core-wall. An overall view of the experimental test set-up is shown in Figure 20, and Figure 21 shows a view of how the core-wall specimen was loaded with four 1000 kN actuators.

Figure 20: Core-wall test overall view

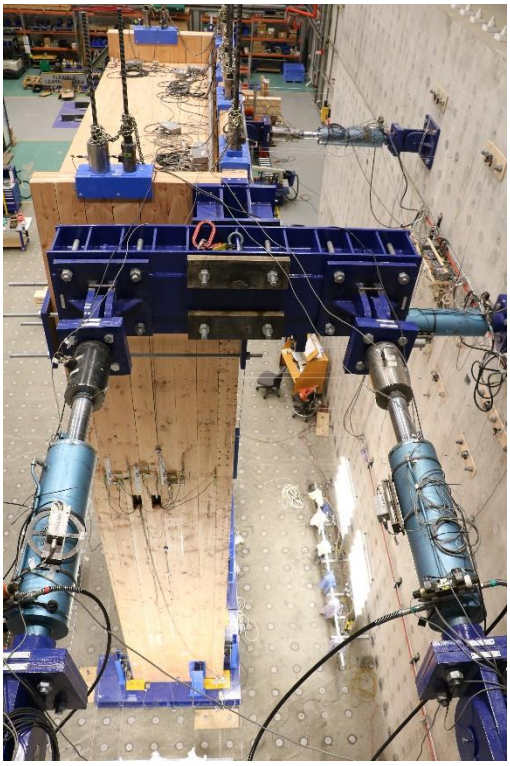

Figure 21: Loading view

3 ANALYTICAL STRENGTH PREDICTIONS

Analytical strength predictions were carried out for each experimental test. These strength predictions were determined based on simplified analytical models in addition to consultation with design engineers.

3.1 Screwed Connection Testing

Bejtka and Blaß (2002) exploited the high tensile capacity of STS in glued laminated timber by installing inclined screws such that the ultimate load on the joints was not only limited by the embedding strength of the timber member and bending capacity of the fastener, but also the withdrawal capacity of the fastener and friction between the timber members. An equation was proposed for inclined STS in single shear connections and it was shown that if the inclination of the screw is greater than 30 degrees, the ultimate withdrawal capacity of the screw and hence maximum efficiency could be reached. Since then, other research programs have explored inclined angle screw connections. Tomasi, Crosatti and Piazza (2010) tested inclined STS in glued laminated timber and concluded that while increasing angles up to 45 degrees will provide large increases in strength and stiffness, the connection ductility will be decreased.

In an effort to address the adverse effect of decreased ductility in inclined screw connections, Piazza et al.(2011) and Tomasi et al. (2006) found that by installing both inclined screws and orthogonal screws in the connection, it is possible to achieve ductile behavior of the STS connections.

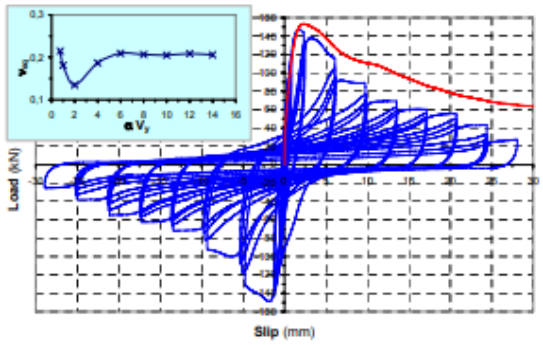

Figure 22: Inclined screw tests (Piazza et al., 2011)

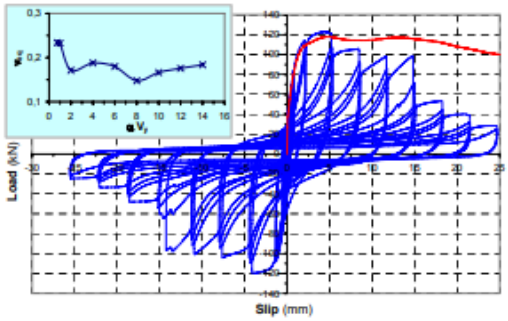

Figure 23: Mixed angle screw tests (Piazza et al., 2011)

In this project, strength predictions were made by neglecting friction between timber members and only considering the force component of the axially loaded screws in the loading direction. According to previous research, this would under predict the actual strength of the connections. However, neglecting friction is a standard practice in industry.

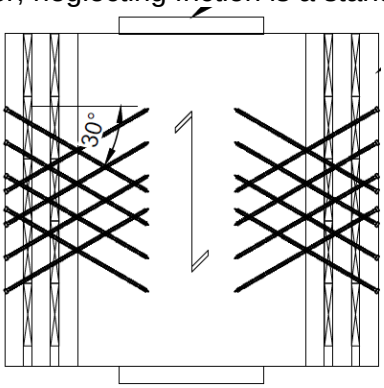

Figure 24: Screw testing angle

For the connection in Figure 24, the connection strength can be derived from as follows.

$F_v = F_{ax} * \sin(\beta)$ (kN), where $90 - \alpha = \beta = 30°$

The withdrawal strength, F_{ax}, varies depending on the method you choose in literature and building code.

The most common methods for determining the withdrawal strength are provided in Eurocode5 (CEN, 2004), the CLT Handbook (Gagnon, Pirvu, & Fpinnovations, 2011), or the SPAX ETA report (ETA, 2012), and these equations are shown in respective order below.

$$F_{ax,\alpha,k} = n_{ef} * 0.52 * d^{-0.5} * l_{ef}^{-0.1} * \rho_k^{0.8} * d * l_{ef} * \left(\frac{\rho_k}{350}\right)^{0.8} * \left(\frac{1}{1.2*(\cos\alpha)^2+(\sin\alpha)^2}\right) \ (N)$$ (CEN, 2004)

$$F_{ax,\alpha,k} = 0.35 * d^{0.8} * {l_{ef}}^{0.9} * {\rho_k}^{0.75} * \left(\frac{1}{1.5*(\cos\alpha)^2+(\sin\alpha)^2}\right) \ (N)$$ (Gagnon et al., 2011)

Where α = 90° for screws installed on the panel face and 0° for screws installed on the panel edge.

$$F_{ax,\alpha,k} = n_{ef} * f_{ax,k} * d * l_{ef} * \left(\frac{\rho_k}{350}\right)^{0.8} * \left(\frac{1}{1.2*(\cos\alpha)^2+(\sin\alpha)^2}\right) \ (N)$$ (ETA, 2012)

Where $f_{ax,k}$ is 12.0 N/mm^2 for ø8mm screws and 11.0 N/mm^2 for ø12mm screws.

Strength predictions of screwed connections with inclined angles are ongoing research topics and there are no conclusive equations. Strength predictions with screws installed with 90 degrees can follow the European Yield Model for timber to timber connections, as provided in Eurocode5 (CEN, 2004). The embedment strength parameters was chosen following the CLT Handbook

(Gagnon et al., 2011). Compression screws were assumed to behave similar to those screws installed 90 degrees to the panel. Table 8 gives the design strength predictions of the screwed connections of different connection setup. Following Eurocode 5, the predictions adopted k_{mod} = 1.1 and γ_m = 1.3.

Table 8: Screwed connection testing strength prediction

	CLT5					*CLT7*		
Name	400X	200X	16X+16	8T	8C	375X	12X+4	12X+6
EC5 (kN)	106	68	127.2	40	28	105	136	151
CLT Handbook (kN)	72	51	110	22	28	95	125	140
Spax ETA (kN)	97	61	120	32	28	104	134	149

3.2 Castellated Connection Testing

Very little research has been conducted on castellated connections and current design equations for these connections in CLT are based on conservative assumptions. Schmidt and Blaß (2016, 2017) have recently researched and tested castellated joints in CLT with the focus on testing the connections loaded along the longitudinal direction of laminations in outer layer. Therefore, the capcaity of the connections is governed by longitudinal shear of the wood laminations. Figure 25 shows the connection is loaded perpendiclular to grain of the face laminations. Figure 26 shows the connections is loaded parallel to grain of the face laminations. The strength prediction methods are different for these two different scenarios.

Figure 25: Load perpendicular to outer CLT layer

Figure 26: Load parallel to outer CLT layer

3.2.1 Load perpendicular to grain of outer CLT layer

When loaded perpendicular to grain of the outer layer, rolling shear is assumed to govern the load carrying capacity, and this assumption has been adopted by engineers in practical design. Previous research at UC funded by SWP has experimentally evaluated rolling shear properties of Douglas-Fir CLT and the experimental results were used for the strength predictions of the connection specimens, as shown in Table 9.

Table 9: Douglas-fir CLT rolling shear capacity

	Lamination Thickness		
	20mm	35mm	45mm
5^{th} percentile (MPa)	2.21	1.12	0.94
Mean (MPa)	2.84	1.6	1.35

With reference to Figure 27 and CLT5, the prediction calculation would be as follows:

$$F_v = f_{rs} * t * h * n_{planes} * n_{joints} \, (kN)$$

Thus, the strength predictions for the tests with configurations C1 and C2 in CLT5 and CLT7 are shown in Table 10.

Table 10: Load perpendicular to outer CLT layer strength prediction

	C1	*C2*
CLT5	56 kN	38 kN
CLT7	85 kN	56 kN

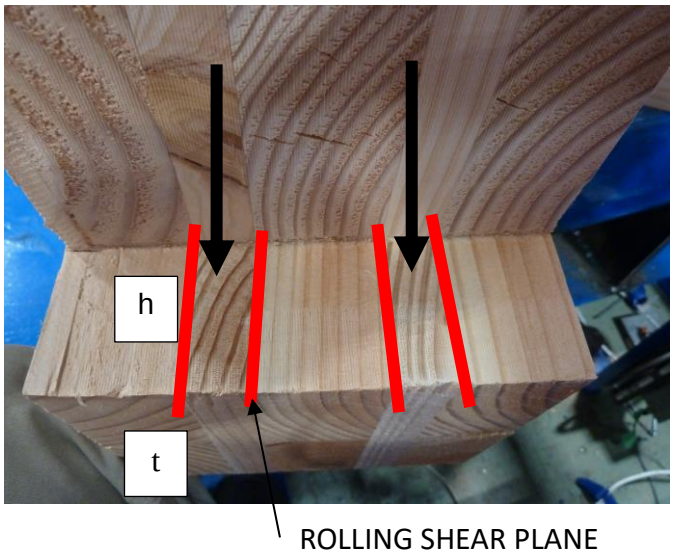

Figure 27: Perpendicular load transfer mechanism

3.2.2 Load parallel to grain of outer CLT layer

When loaded parallel to grain of the outer CLT layer, longitudinal shear strength of the timber laminations are used. As no experimental data of Douglas-fir laminations is available, previous experimental data of Radiata pine timber was used as a reference to derive the longitudinal shear strength of Douglas-fir for the strength predictions. Table 11 lists the used strength values.

Table 11: Radiata Pine CLT longitudinal shear capacity

	Strength Value
Characteristic design value Radiata Pine, Douglas-fir (MPa)	3.8, 3.0
95^{th} percentile (MPa)	8.6
Mean (MPa)	7
5^{th} percentile (MPa)	5.8

With reference to Figure 26, the prediction calculation would be as follows:

$$F_v = f_{ls} * t * thickness_{long.layer} * n_{parallel\ layers} * n_{joints}\ (kN)$$

Thus, the strength predictions for the test configurations C3 and C4 in CLT5 and CLT7 (Table 4) are shown in Table 12.

Table 12: Load parallel to outer CLT layer strength prediction

		C3	*C4*
CLT5	95th percentile	244 kN	174 kN
	Mean	199 kN	141 kN
	5th percentile	164 kN	117 kN
CLT7	95th percentile	289 kN	206 kN
	Mean	235 kN	168 kN
	5th percentile	195 kN	140 kN

3.3 Core-wall System Testing

The core-wall system testing consisted of both a post-tensioned rocking wall system and a conventional system. The strength predictions for each type of system is described below.

3.3.1 Post-tensioned walls (or Pres-Lam walls)

Starting in 2005, Post-tensioned timber or Pres-Lam research program began at University of Canterbury (Palermo, Pampanin, Buchanan, & Newcombe, 2005). The Pres-Lam system was adopted from the PRESS precast concrete system which was developed at the University of California (Pampanin, 2005; Priestley, 1991). In the Pres-Lam system, structural elements are connected by unbonded post-tensioning bars or tendons such that seismic demand can be accommodated by controlled rocking of the timber frame or wall (Palermo, Pampanin, Fragiacomo, Buchanan, & Deam, 2006). Hybrid Pres-Lam systems include both unbonded post-tensioning and energy dissipating devices such as U-shaped flexural plates (UFPs) (Iqbal, Pampanin, Palermo, & Buchanan, 2015; Kelly, Skinner, & Heine, 1972). Experimental studies on the Pres-Lam system included rocking frames and walls, staircase cores and floor-diaphragm connections (Dunbar, 2014; Moroder, 2016; Newcombe, 2011; Sarti, 2015; Smith, 2014). Small scale testing on post-tensioned wall assemblies was mainly focused on LVL walls (Palermo, Pampanin, & Buchanan, 2006). Today, the Pres-Lam system has many built examples such as the NMIT building (Devereux, Holden, Buchanan, & Pampanin) in Nelson which uses coupled LVL walls with UFP dissipaters. A detailed design guide has been published as a result of the extensive research programme (Pampanin, Palermo, & Buchanan, 2013). The design guide provides analytical equations to calculate the wall strength at target drift levels. At each drift level, there is moment equilibrium that must be achieved at the base of the wall. As shown in Figure 28, the unbonded post-tensioning bar force (T_{pt}) due to gap opening and the timber compression force (C_t) create the moment couple. In order to determine C_t, the Modified Monolithic Beam Analogy (MMBA) is used to determine the strain in the timber.

$$\epsilon_t = c(3\frac{\theta_{imp}}{L_{cant}} + \varphi_{dec})$$

Where:

$$\epsilon_t = timber\ strain, c = length\ of\ neutral\ axis, \theta_{imp} = imposed\ rotation\ at\ wall\ base, L_{cant} = cantilevered\ length\ of\ wall, \varphi_{dec} = decompression\ curvature$$

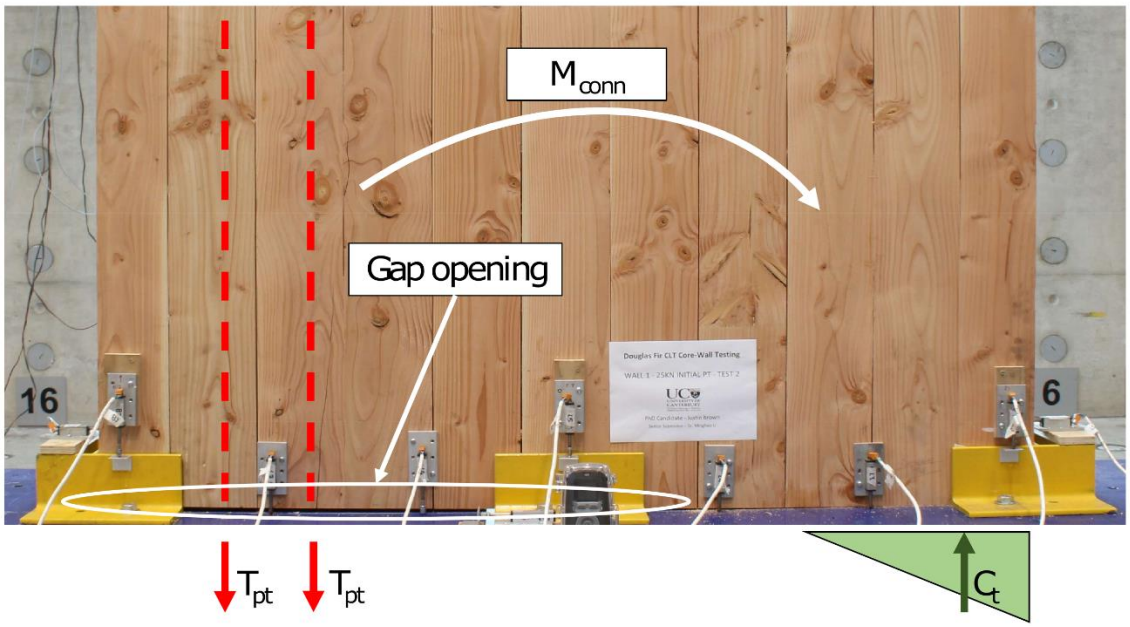

Figure 28: Rocking wall behavior

Following the timber guide, the upper bound strength predictions of the single wall, coupled wall, and core-wall system can be made. Figure 29 shows the predictions of the single wall.

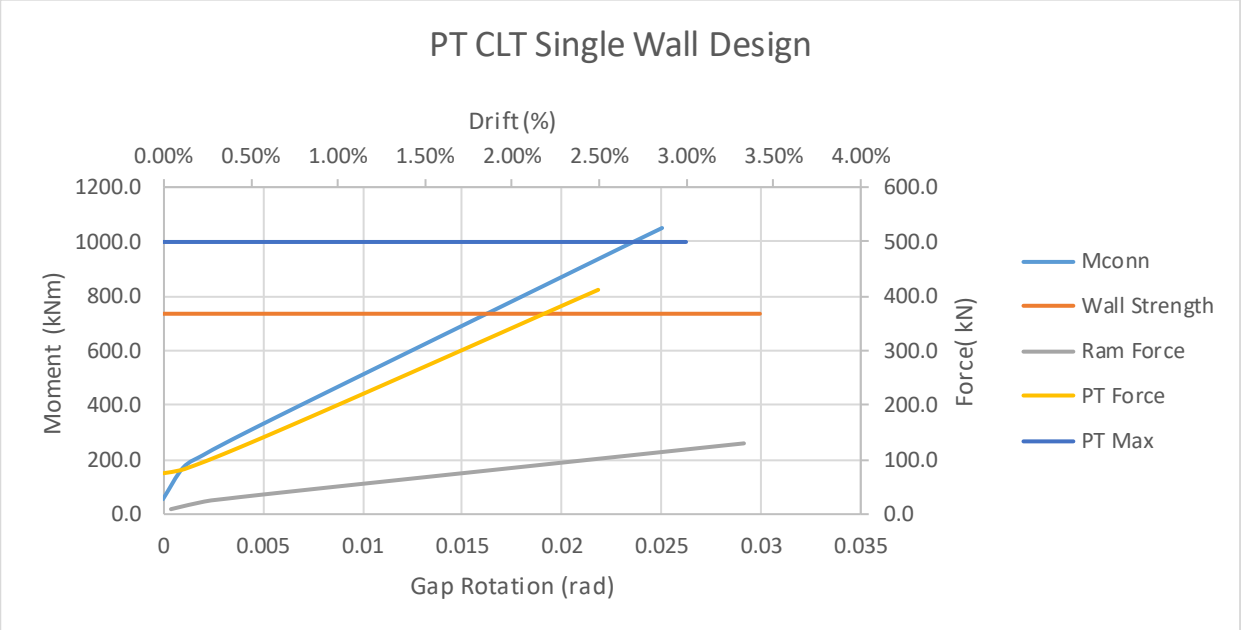

Figure 29: Single wall strength prediction

Figure 30 below shows the strength prediction assuming a completely rigid joint between wall 1 and 2.

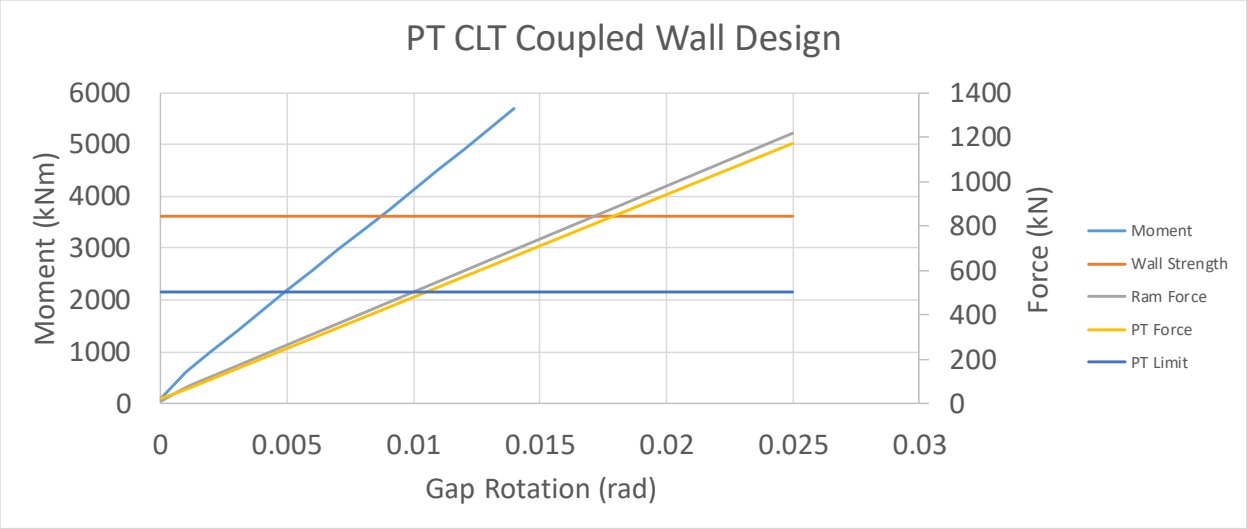

Figure 30: Coupled wall strength prediction

Figure 31 shows the predicted loads assuming completely rigid joints between all wall panels and the post-tensioned bar force (yellow curve) would govern the design with a yield force of 400kN. Thus, the maximum actuator load predicted was approximately 1200kN, and this was the governing load used for design of the specimen at about 2% drift ratio.

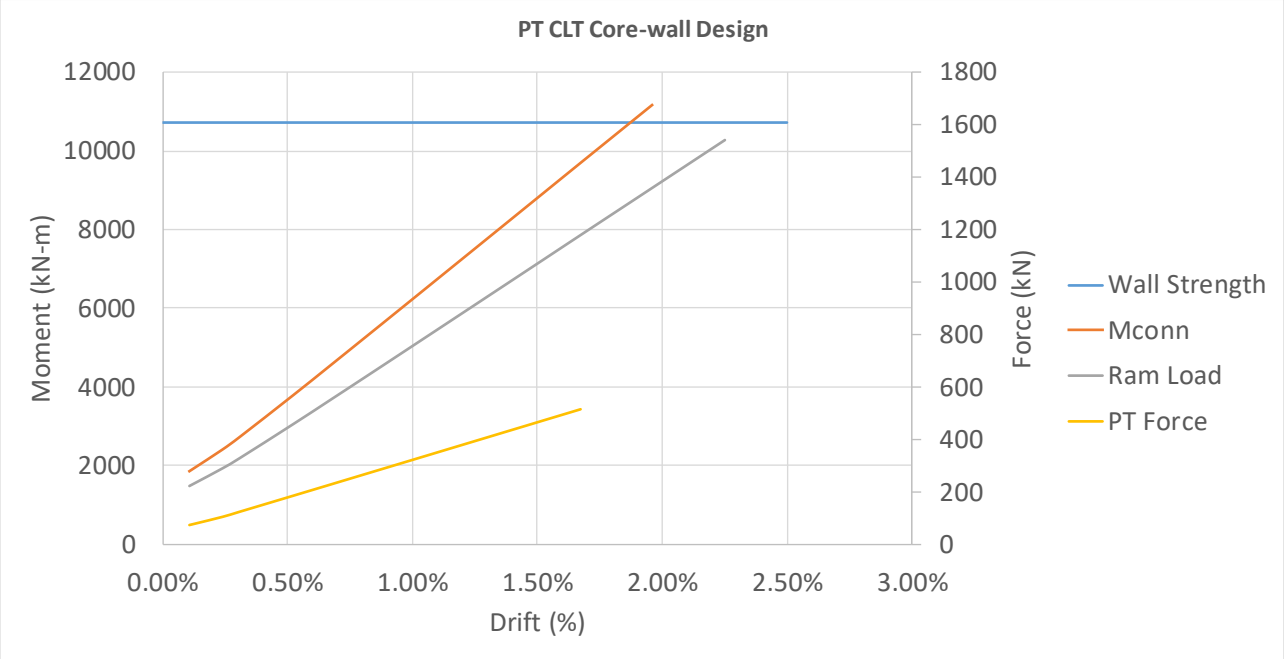

Figure 31: Core-wall strength prediction

As no previous research has been done to accurately quantify the contribution from orthogonal walls, which heavily replies on the stiffness and strength of the connection systems, the upper bound strength predictions shown above were used.

3.3.2 Conventional core-wall strength prediction

In conventional CLT wall design, the connections to the foundation typically govern the design. Dujic, Pucelj, and Zarnic (2004) tested the lateral resistance of two dimensional CLT walls under racking loads. Monotonic and cyclic tests were performed to assess the in plane stiffness and the influence of standard steel angle connectors. The tests concluded that connections were the weakest links of the system. Under the SOFIE project in Italy, Dujic, Aicher and Zarnic (2005) studied the in-plane behaviour of CLT shear walls as well and concluded that the behaviour of the walls was strongly influenced by the connections.

(Gavric, Fragiacomo, & Ceccotti, 2015) developed analytical prediction models and compared them to past experimental tests. Figure 32 shows how the overall behaviour of in-plane CLT walls is governed by the connections' stiffness, strength, and displacement capacity. In particular, the hold-down connections stiffness's $k_{1,I}$ and $k_{2,I}$ are critical parameters.
In this study, hold-downs with mixed angle screws, shown in Figure 33, were used in the conventional core-wall testing as the previous screwed connection test results indicated the improved ductile performance of screws installed with mixed angles.

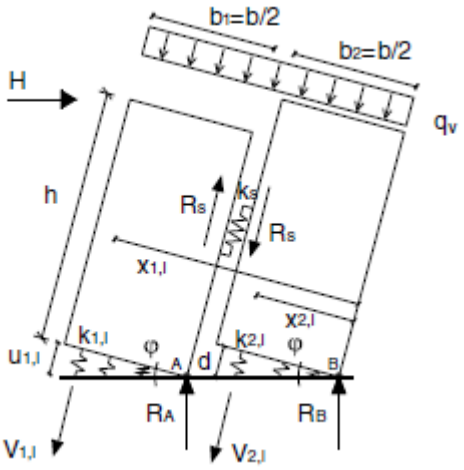

Figure 32: Schematic of coupled CLT wall panel behavior (Gavric et al., 2015)

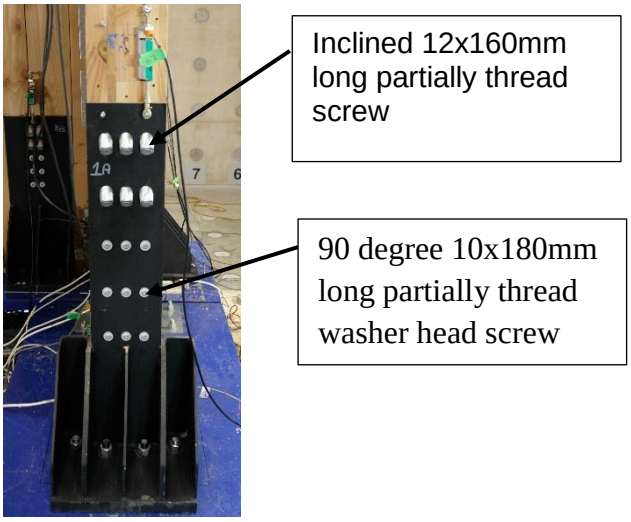

Figure 33: Mixed angle screwed hold-down

Because the stiffness, strength and displacement capacity of these new screwed hold-downs have not been well researched, a robust strength prediction is very difficult. Therefore, capacity design was used to ensure that the ductile failure mechanism would be observed in the hold-downs. For all the hold-downs, the intended failure mechanism is gradual screw withdrawal from CLT panels and this is much more ductile failure mode compared with the brittle tensile failure of screws. Titan TCN240 base shear keys were installed to resist maximum base shear load of 380kN.

4 EXPERIMENTAL RESULTS

This section presents the experimental results of the connection tests and the wall tests. The derivation of the connection properties such as yield strength, stiffness and ductility ratios followed the equivalent energy elastic-plastic (EEEP) method (ASTM International, 2011).

4.1 Screwed Connection Testing

The experimental curves and results for each testing series are shown in the tables and graphs below.

Table 13: CLT5-400X test series results summary

Series	*400X*									
Test	M1	M2	M3	Average	C1	C2	C3	C4	C5	Average
$F_{pred.}$ *(kN)*	106	106	106	106	106	106	106	106	106	106
F_y *(kN)*	183.5	179.0	205.4	189.3	176.2	186.2	176.8	176.2	162.2	175.5
F_{max} *(kN)*	200.5	206.8	217.2	208.2	206.4	211.8	196.8	202.2	192.9	202.0
F_u *(kN)*	160.4	165.4	173.8	166.5	165.1	169.4	157.4	161.7	154.3	161.6
Δ_y *(mm)*	4.7	2.4	3.7	3.6	2.7	2.6	2.7	2.3	1.8	2.4
Δ_{max} *(mm)*	6.5	5.6	5.8	6.0	5.3	5.1	5.4	4.8	4.5	5.0
Δ_u *(mm)*	8.3	5.6	7.4	7.1	7.0	5.9	6.1	5.9	5.0	6.0
K (kN/mm)	39.3	74.6	54.9	56.3	67.0	73.7	65.8	82.4	88.7	75.5
μ	1.8	2.3	2.0	2.0	2.7	2.3	2.3	2.5	2.8	2.5
Mode	LD	LD	LD	LD	LD	LD	LD	LD	LD	LD

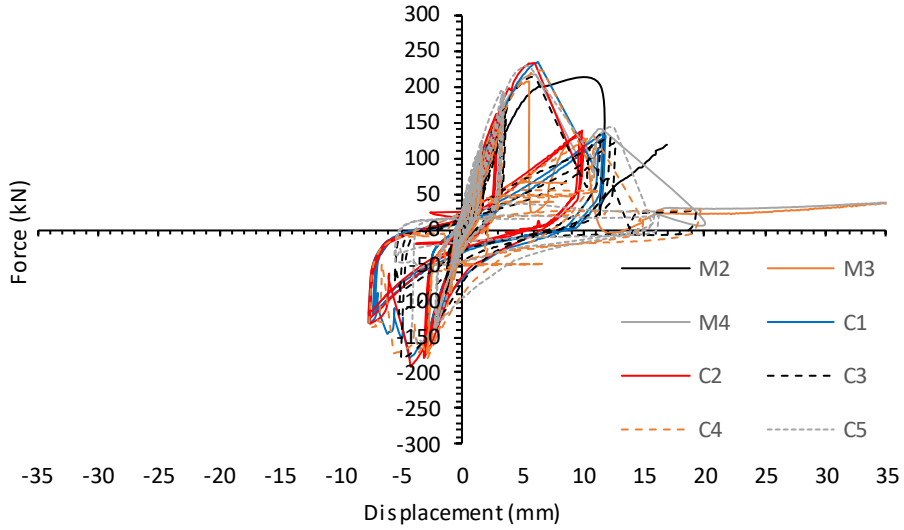

Figure 34: CLT5-400X test series

Table 14: CLT5-200X test series results summary

Series	*200X*									
Test	M1	M2	M3	Average	C1	C2	C3	C4	C5	Average
$F_{pred.}$ *(kN)*	68	68	68	68	68	68	68	68	68	68
F_y *(kN)*	148.6	120.0	171.4	146.7	151.9	149.3	152.4	152.1	150.2	151.2
F_{max} *(kN)*	164.8	135.0	187.8	162.5	168.8	161.0	171.1	171.8	168.2	168.1
F_u *(kN)*	131.8	108.0	150.2	130.0	135.0	128.8	136.8	137.4	134.5	134.5
Δ_y *(mm)*	2.1	1.2	1.7	1.7	1.6	1.6	1.6	2.0	1.9	1.7
Δ_{max} *(mm)*	5.9	8.6	5.1	6.5	5.1	4.4	4.9	5.4	5.3	5.0
Δ_u *(mm)*	10.5	13.0	9.6	11.1	8.2	6.5	8.9	9.2	8.3	8.2
K (kN/mm)	71.6	102.4	99.1	91.0	97.7	99.4	92.8	81.4	79.8	90.2
μ	5.1	11.1	5.6	7.3	5.0	4.2	5.5	4.8	4.4	4.8
Mode	MD	D	MD	D	MD	MD	MD	MD	MD	MD

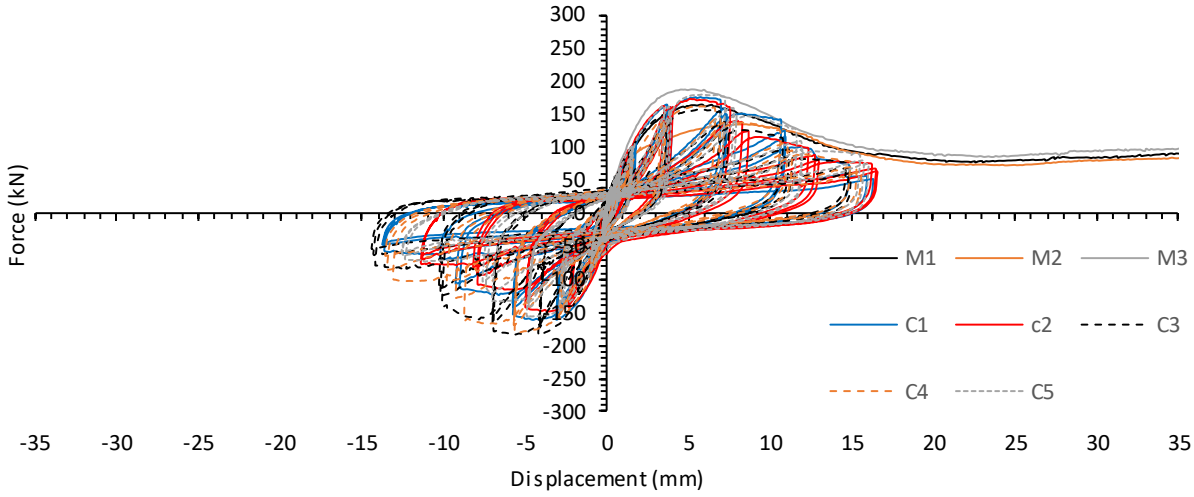

Figure 35: CLT5-200X test series

Table 15: CLT5-16X+16 test series results summary

Series	*16X+16*									
Test	M1	M2	M3	Average	C1	C2	C3	C4	C5	Average
$F_{pred.}$ *(kN)*	127.2	127.2	127.2	127.2	127.2	127.2	127.2	127.2	127.2	127.2
F_y *(kN)*	258.7	270.3	259.3	262.8	203.9	196.9	199.4	199.5	192.9	198.5
F_{max} *(kN)*	298.7	324.3	316.8	313.3	247.9	232.7	244.4	235.2	229.1	237.8
F_u *(kN)*	239.0	259.4	253.4	250.6	198.3	186.2	195.5	188.1	183.3	190.3
Δ_y *(mm)*	2.2	2.8	2.7	2.6	1.7	1.9	1.9	1.7	1.8	1.8
Δ_{max} *(mm)*	21.6	23.2	22.5	22.5	10.6	10.7	22.9	5.6	5.3	11.0
Δ_u *(mm)*	30.5	30.9	28.5	30.0	18.3	26.1	30.1	18.1	18.0	22.1
K (kN/mm)	118.8	96.5	96.2	103.8	119.2	105.4	108.1	116.3	107.8	111.4
μ	14.0	11.0	10.6	11.9	10.7	14.1	16.3	10.7	10.0	12.3
Mode	D	D	D	D	D	D	D	D	D	D

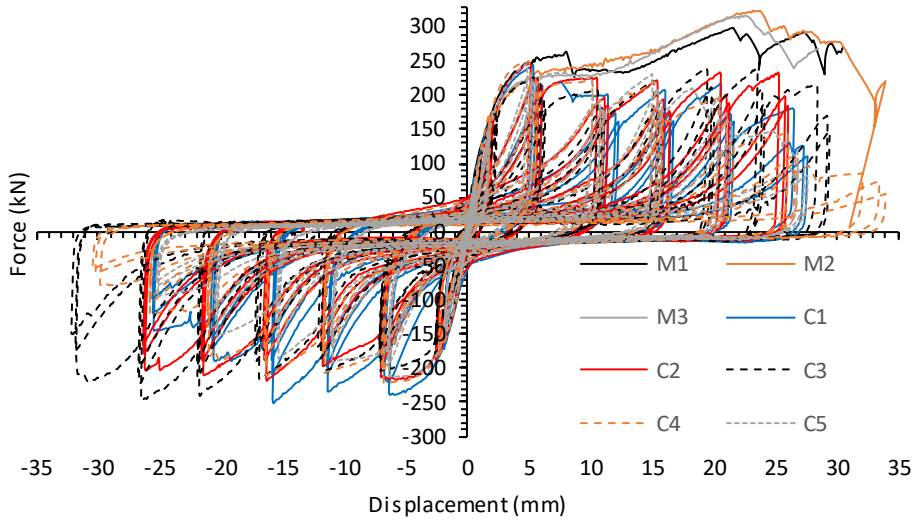

Figure 36: CLT5-16X+16 test series

Table 16: CLT5-8T & 8C test series results summary

Series	*8T*				*8C*			
Test	M1	M2	M3	Average	M1	M2	M3	Average
$F_{pred.}$ *(kN)*	40	40	40	40	28	28	28	28
F_y *(kN)*	127.1	125.9	129.0	127.3	46.7	42.2	40.5	43.1
F_{max} *(kN)*	137.9	135.9	140.2	138.0	76.3	67.4	76.0	73.2
F_u *(kN)*	110.3	108.7	112.2	110.4	61.1	53.9	60.8	58.6
Δ_y *(mm)*	2.3	2.1	3.6	2.6	2.8	2.9	3.1	2.9
Δ_{max} *(mm)*	5.8	5.7	6.5	6.0	40.1	45.1	33.6	39.6
Δ_u *(mm)*	9.6	10.6	12.9	11.1	40.1	45.1	38.2	41.1
K (kN/mm)	55.6	60.4	36.3	50.7	16.4	14.8	12.9	14.7
μ	4.2	5.1	3.6	4.3	14.1	15.8	12.2	14.0
Mode	MD	MD	LD	MD	D	D	D	D

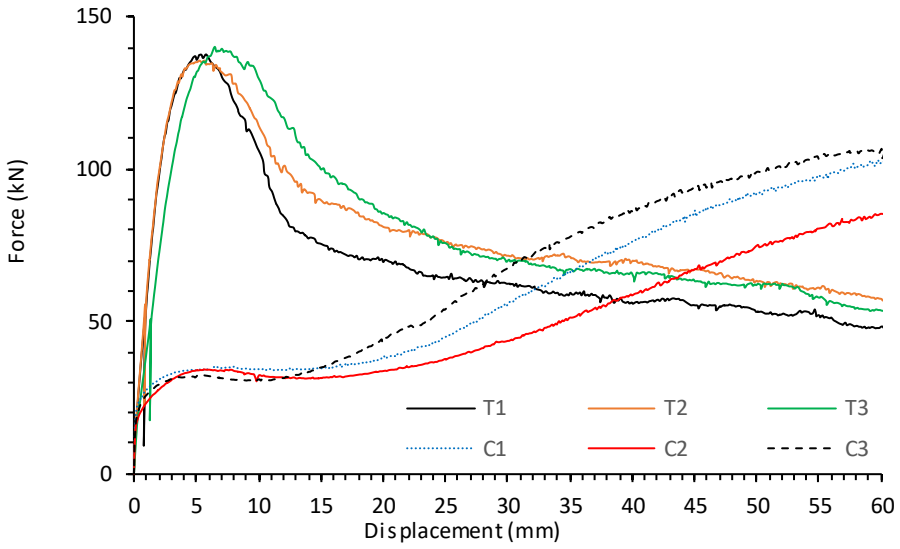

Figure 37: 8T and 8C test series

Table 17: CLT7-375X test series results summary

Series	*375X*									
Test	M1	M2	M3	Average	C1	C2	C3	C4	C5	Average
$F_{pred.}$ *(kN)*	105	105	105	105	105	105	105	105	105	105
F_y *(kN)*	211.3	200.5	188.7	200.2	189.3	225.4	229.9	222.9	223.7	218.2
F_{max} *(kN)*	233.8	214.9	209.5	219.4	213.9	251.0	258.1	248.8	244.7	243.3
F_u *(kN)*	187.0	171.9	167.6	175.5	171.1	200.8	206.4	199.0	195.8	194.6
Δ_y *(mm)*	2.0	1.9	1.5	1.8	1.6	1.7	1.8	1.9	1.5	1.7
Δ_{max} *(mm)*	6.9	5.5	5.3	5.9	7.0	5.4	5.1	5.6	5.5	5.7
Δ_u *(mm)*	15.0	14.8	19.3	16.4	15.9	10.7	10.1	10.0	10.9	11.5
K (kN/mm)	106.9	105.0	126.9	112.9	115.8	134.9	128.8	119.6	149.6	129.7
μ	7.6	7.8	13.0	9.4	9.6	6.2	5.6	5.4	7.1	6.8
Mode	D	D	D	D	D	D	MD	MD	D	D

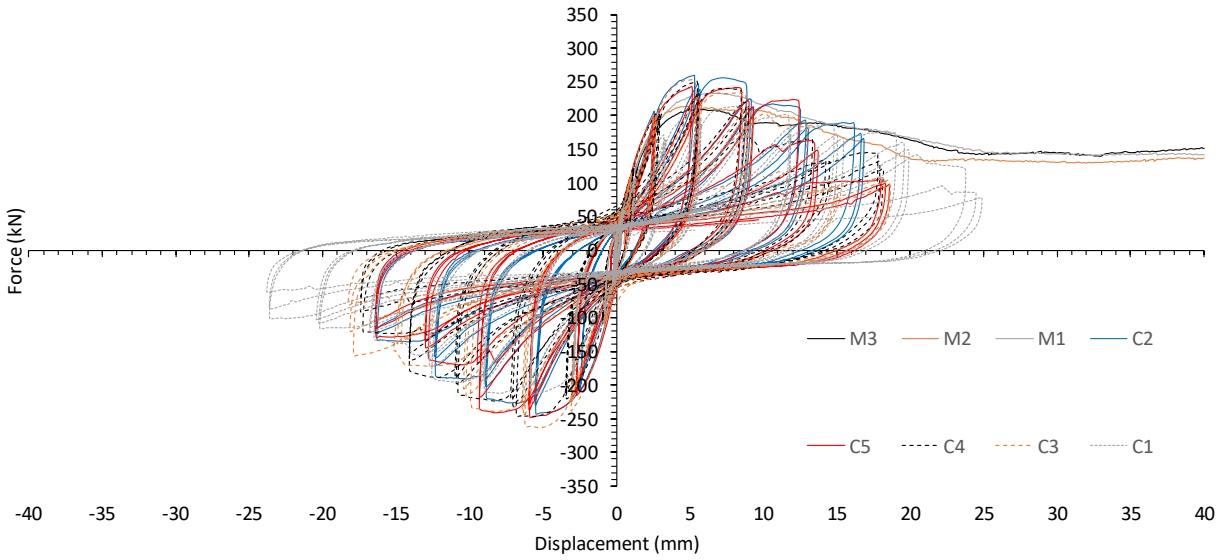

Figure 38: CLT7-375X test series

Table 18: CLT7-12X+4 test series results summary

Series	*12X+4*									
Test	M1	M2	M3	Average	C1	C2	C3	C4	C5	Average
$F_{pred.}$ *(kN)*	136	136	136	136	136	136	136	136	136	136
F_y *(kN)*	273.4	297.1	279.6	283.4	282.3	285.1	249.7	280.6	274.1	274.4
F_{max} *(kN)*	292.9	322.6	345.1	320.2	319.2	316.1	281.7	316.4	309.2	308.5
F_u *(kN)*	234.3	258.1	276.1	256.2	255.4	252.8	225.4	253.1	247.4	246.8
Δ_y *(mm)*	1.8	2.3	2.6	2.2	2.0	2.0	1.8	1.6	1.9	1.9
Δ_{max} *(mm)*	7.4	39.3	68.2	38.3	6.6	6.8	6.6	5.4	7.5	6.6
Δ_u *(mm)*	38.2	51.3	69.6	53.0	13.6	12.4	13.9	11.4	16.4	13.5
K (kN/mm)	152.8	127.5	108.5	129.6	138.8	139.1	142.5	176.0	146.7	148.6
μ	21.4	22.0	27.0	23.4	6.7	6.1	8.0	7.1	8.8	7.3
Mode	D	D	D	D	D	D	D	D	D	D

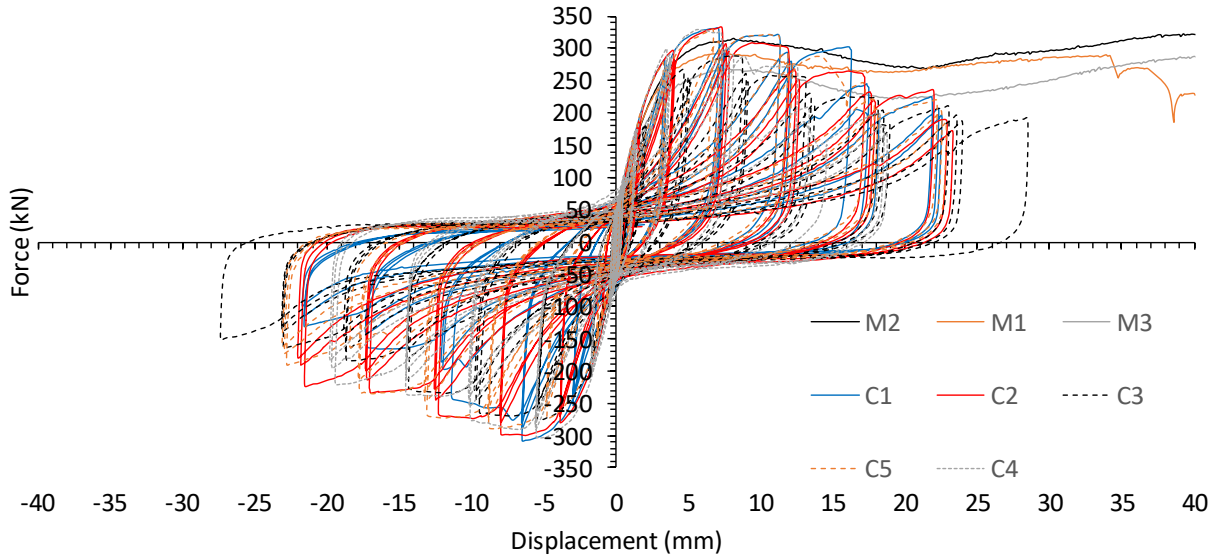

Figure 39: CLT7-12X+4 test series

Table 19: CLT7-12X+6 test series results summary

Series	*12X+6*									
Test	M1	M2	M3	Average	C1	C2	C3	C4	C5	Average
$F_{pred.}$ *(kN)*	151	151	151	151	151	151	151	151	151	151
F_y *(kN)*	357.0	312.7	333.0	334.2	300.3	264.6	251.2	279.6	262.3	271.6
F_{max} *(kN)*	404.8	361.7	387.1	384.5	335.3	302.7	291.3	316.4	321.9	313.5
F_u *(kN)*	323.8	289.4	309.7	307.6	268.2	242.2	233.0	253.1	257.5	250.8
Δ_y *(mm)*	3.8	2.6	2.1	2.8	1.8	1.4	1.3	1.6	1.3	1.5
Δ_{max} *(mm)*	42.7	42.7	39.6	41.7	10.7	8.1	8.7	8.7	10.5	9.4
Δ_u *(mm)*	51.3	54.1	50.8	52.1	14.7	29.5	25.3	20.2	28.2	23.6
K (kN/mm)	94.4	119.4	159.2	124.3	172.2	187.8	187.7	173.9	199.4	184.2
μ	13.6	20.7	24.3	19.5	8.7	21.1	18.7	12.6	21.4	16.5
Mode	D	D	D	D	D	D	D	D	D	D

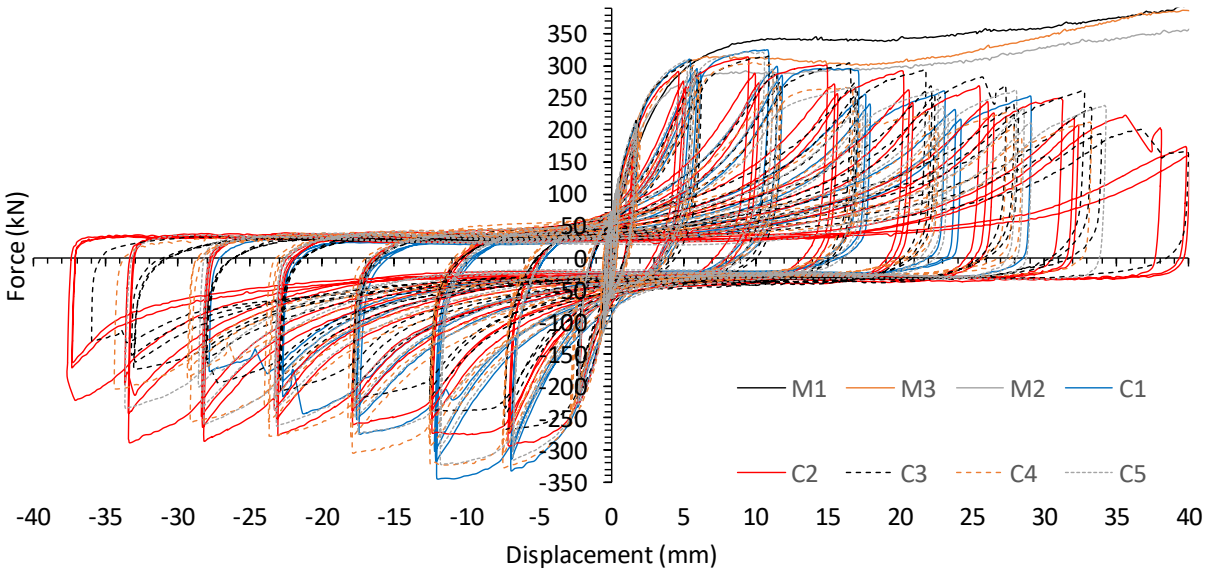

Figure 40: CLT7-12X+6 test series

4.2 Castellated Connection Testing

The experimental curves and results for each testing series is shown in the tables and graphs below.

Table 20: C1 test series results summary

Series	*CLT5-C1*				*CLT7-C1*				
Test	M1	M2	M3	Average	M1	M2	M3	Average	M4
$F_{pred.}$ *(kN)*	56.0	56.0	56.0	56.0	85.0	85.0	85.0	85.0	85.0
F_{max} *(kN)*	213.0	228.3	202.2	214.5	303.6	339.8	301.3	314.9	302.9
Δ_{max} *(mm)*	2.9	5.5	3.0	3.8	2.4	2.6	3.2	2.7	3.8
K (kN/mm)	90.4	34.9	88.0	71.1	132.3	91.2	100.4	108.0	99.8

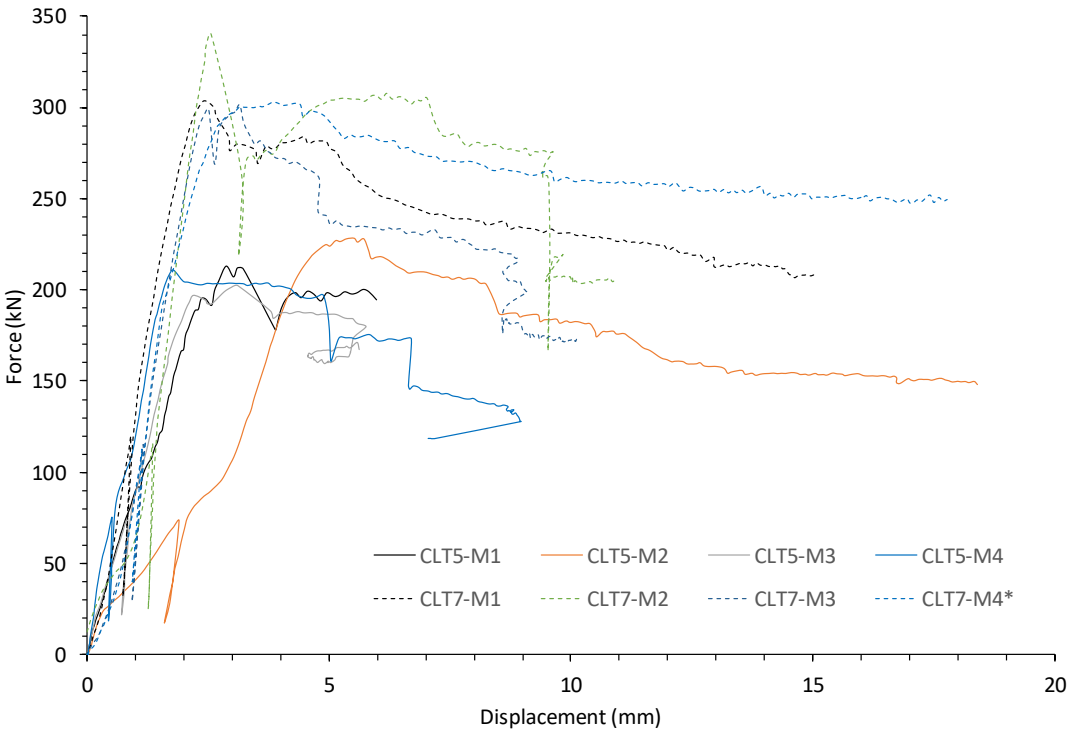

Figure 41: C1 test series

Table 21: C2 test series results summary

Series	*CLT5-C2*					*CLT7-C2*				
Test	M1	M2	M3	Average	M4	M1	M2	M3	Average	M4
$F_{pred.}$ *(kN)*	38.0	38.0	38.0	38.0	38.0	56.0	56.0	56.0	56.0	56.0
F_{max} *(kN)*	136.0	177.9	146.3	153.4	195.9	253.5	249.0	289.9	264.1	278.4
Δ_{max} *(mm)*	21.1	3.0	4.9	9.6	3.4	4.6	5.3	2.9	4.3	3.4
K (kN/mm)	44.6	70.7	32.5	49.3	44.8	74.4	92.8	110.1	92.4	135.7

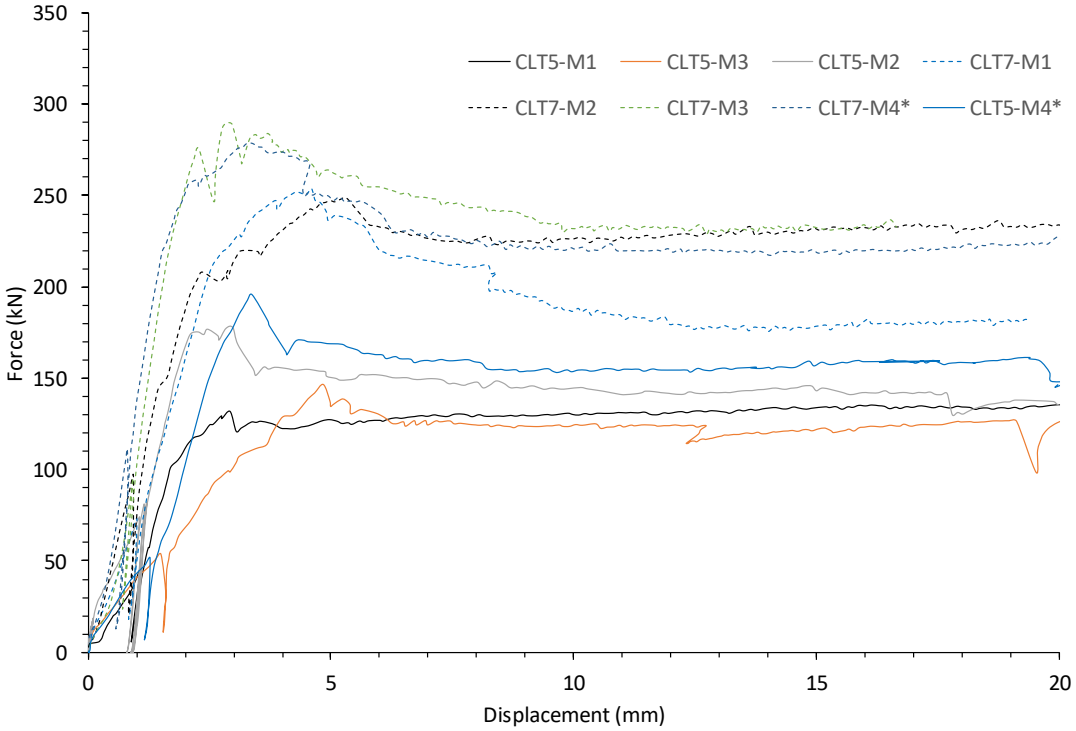

Figure 42: C2 test series

Table 22: C3 test series results summary

Series	*CLT5-C3*					*CLT7-C3*			
Test	M1	M2	M3	Average	M4	M1	M2	M3	Average
$F_{pred.}$ *(kN)*	199.0	199.0	199.0	199.0	199.0	235.0	235.0	235.0	235.0
F_{max} *(kN)*	189.2	169.9	199.7	186.3	232.7	269.2	233.3	237.5	246.7
Δ_{max} *(mm)*	2.1	3.5	3.1	2.9	3.1	1.7	4.9	3.3	3.3
K (kN/mm)	63.1	36.0	46.5	48.5	56.3	124.6	49.5	101.2	91.8

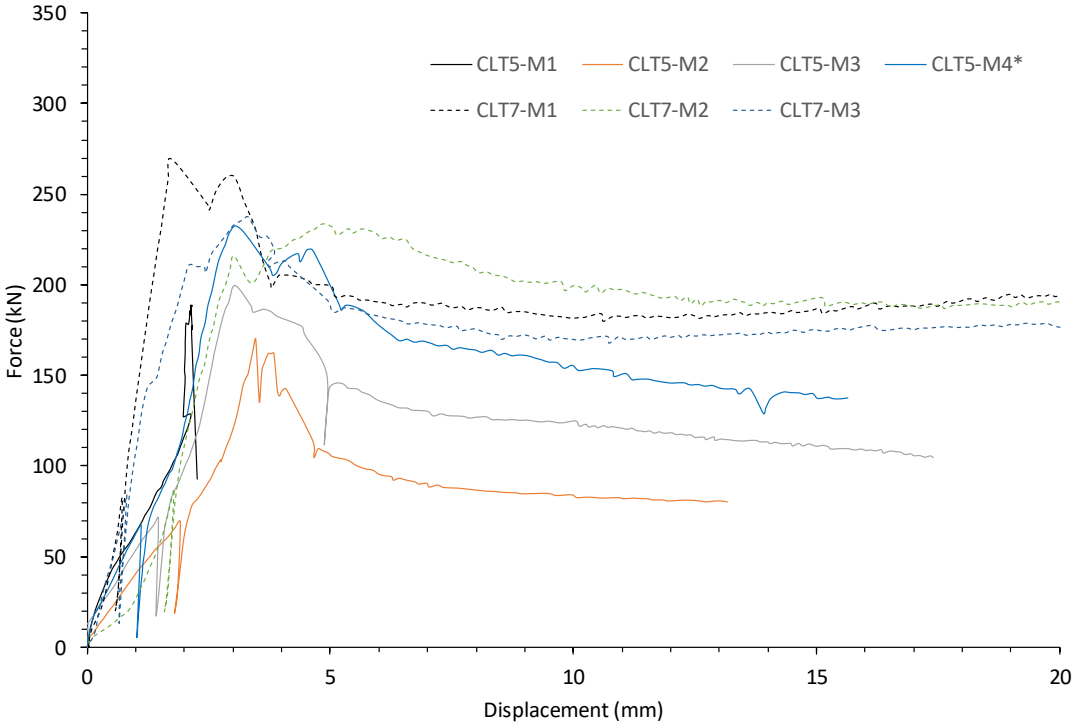

Figure 43: C3 test series

Table 23: C4 test series results summary

Series	*CLT5-C4*					*CLT7-C4*				
Test	M1	M2	M3	Average	M4	M1	M2	M3	Average	M4
$F_{pred.}$ *(kN)*	141.0	141.0	141.0	141.0	141.0	168.0	168.0	168.0	168.0	168.0
F_{max} *(kN)*	123.5	125.0	141.4	130.0	194.8	190.8	200.0	199.0	196.6	173.5
Δ_{max} *(mm)*	5.0	3.2	14.0	7.4	6.7	11.3	6.2	8.5	8.7	5.9
K (kN/mm)	48.3	47.5	47.7	47.8	34.6	35.9	59.8	69.6	55.1	52.7

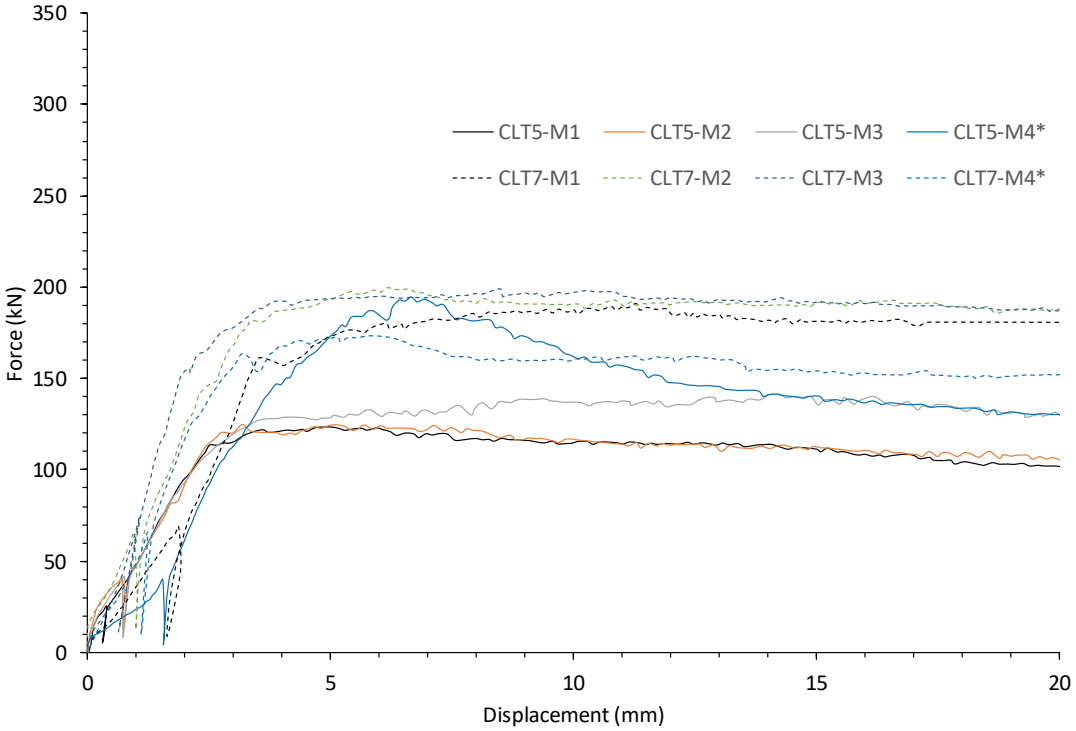

Figure 44: C4 test series

4.3 Core-wall System Testing

The experimental curves and results for each testing series is shown in the tables and graphs below.

4.3.1 Phase I – Single wall testing

Table 24: Single wall testing results summary

Series	Single Wall Testing			
Test	*1*	*2*	*3*	*4*
Initial Post-Tension Force (kN)	*0*	*100*	*200*	*300*
$F_{h/300}$ (kN)	*15.7*	*29.0*	*32.0*	*38.0*
$K_{h/300}$ (kN/mm)	*0.6*	*1.1*	*1.2*	*1.4*
F_u (kN)	*53.4*	*56.7*	*62.6*	*64.3*
Δ_{max} (mm)	*95.0*	*75.9*	*76.0*	*61.1*
Peak Drift	*1.2%*	*0.9%*	*0.9%*	*0.7%*

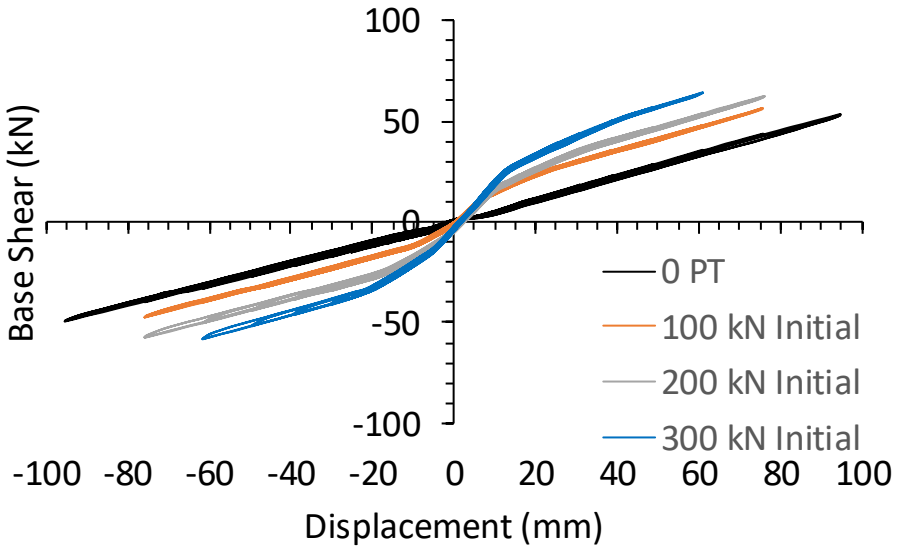

Figure 45: Single wall testing results

4.3.2 Phase II – Coupled wall testing

Table 25: Coupled wall testing results summary

Series	Coupled Wall Testing				
Test	1	2	3	4	5
Initial Post-Tension Force / wall (kN)	100	100	100	100	100
$F_{h/300}$ *(kN)*	45.0	66.0	100.0	71.0	49.0
$K_{h/300}$ *(kN/mm)*	1.6	2.4	3.7	2.6	1.8
F_u *(kN)*	124.4	155.1	216.5	168.9	143.8
Δ_{max} *(mm)*	94.9	94.9	95.0	95.0	94.9
Peak Drift	1.2%	1.2%	1.2%	1.2%	1.2%

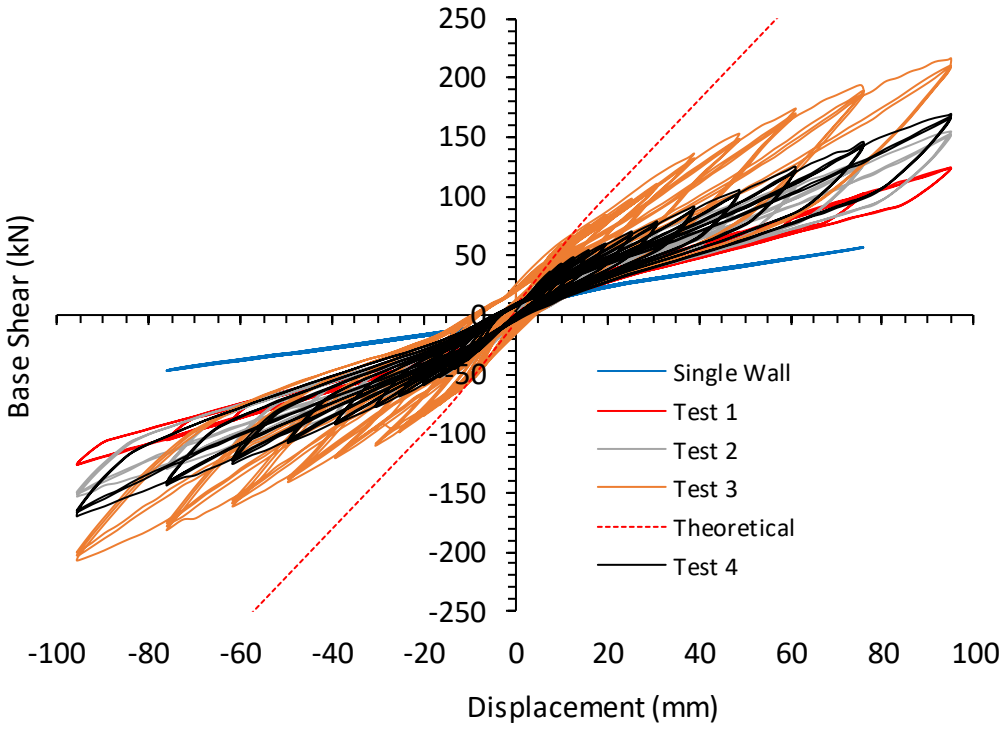

Figure 46: Coupled wall testing results I

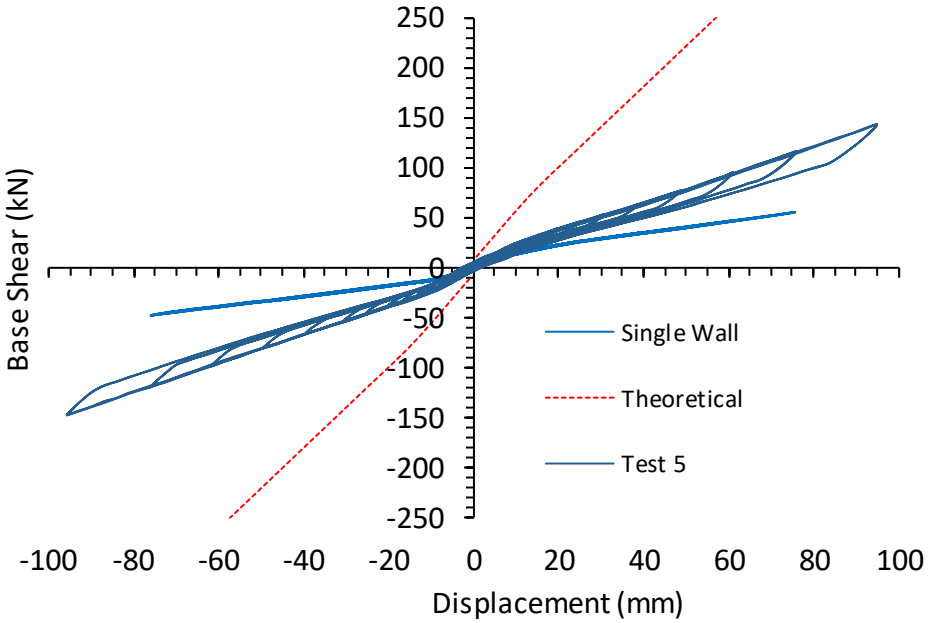

Figure 47: Coupled wall testing results II

4.3.3 Phase III – Core-wall testing

Table 26: Core-wall testing results summary

Series	*Post-tensioned core-wall testing*						
Test	1	2	3	4	5	6	7
Initial Post-Tension Force / bar (kN)	25	75	75	75	75	75	25
Fh/300 (kN)	59.9	179	76.7	76.4	230	242.1	128
Kh/300 (kN/mm)	2.2	6.5	2.8	2.8	8.4	8.9	4.7
Fu (kN)	154.29	375.1	140.06	146.35	554.8	845	460
Δmax (mm)	95.055	119.55	61.45	66.91	95.215	186.25	187.75
Peak Drift	1.2%	1.5%	0.7%	0.8%	1.2%	2.3%	2.3%

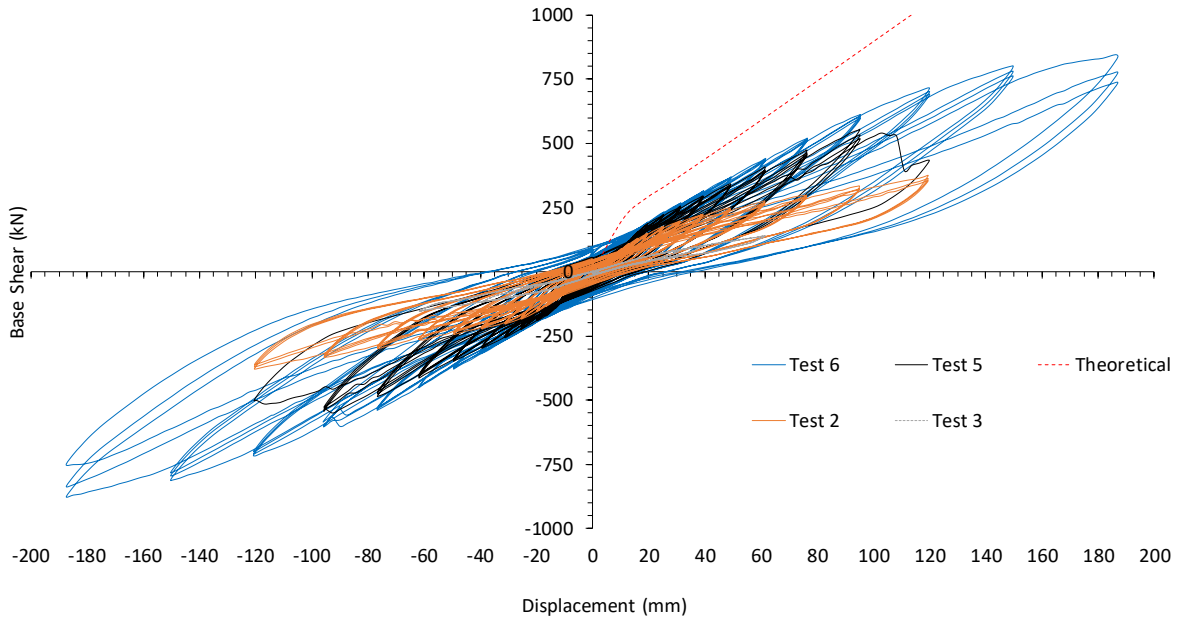

Figure 48: Post-tensioned core-wall testing results

Table 27: Test 8 results summary EEEP

Series	*Test 8 – Conventional Test*
F_y *(kN)*	374
F_{max} *(kN)*	417
F_u *(kN)*	333
Δ_y *(mm)*	62.7
Δ_{max} *(mm)*	151.4
Δ_u *(mm)*	174.6
K (kN/mm)	6.0
μ	2.8
Mode	LD

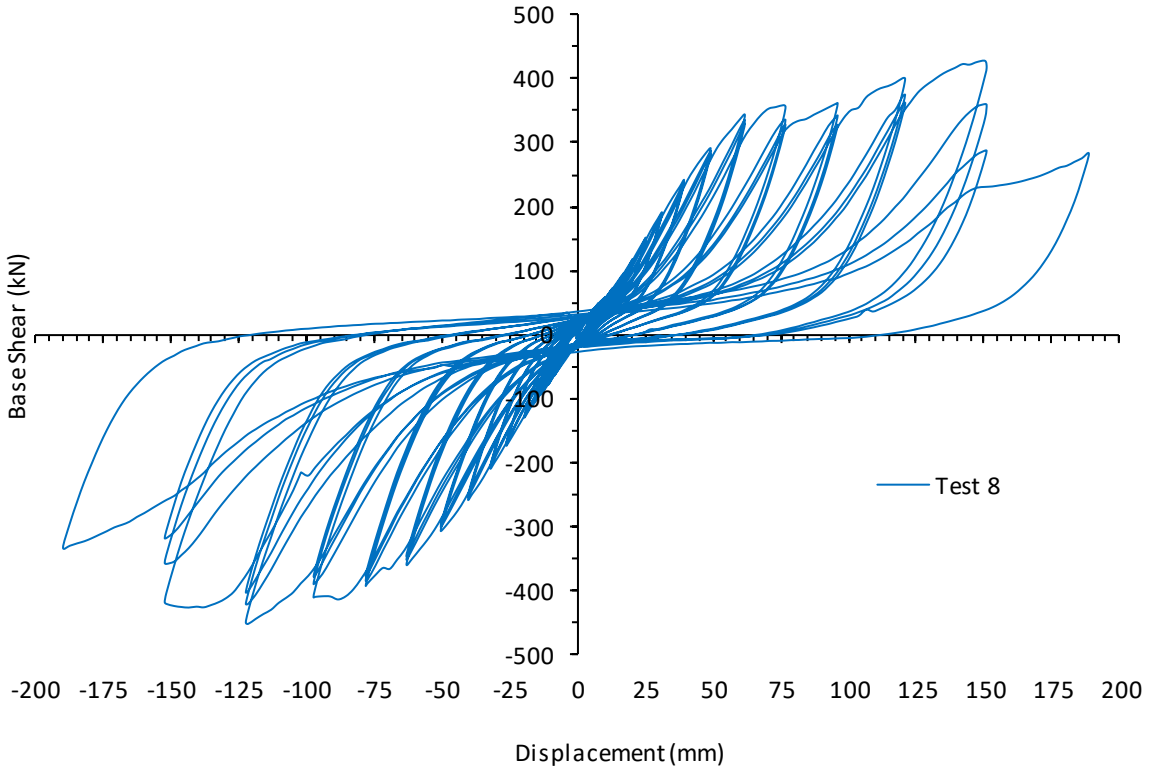

Figure 49: Conventional core-wall testing result

5 DISCUSSION AND CONCLUSIONS

5.1 Screwed Connection Testing

Figure 50 and Figure 51 compare the test results of the screwed connections with different connection details. First, capacity design was used to limit the screw embedment length to ensure the withdrawal failure instead of sudden screw tensile failure would occur. For example, CLT5-400X test series experience sudden brittle failure of the screws due to large embedment length. Another key finding was related to the use of mixed angle screw configurations. The mixed angle screw specimens showed comparable initial stiffness to the inclined screws but significantly higher displacement capacity and ductility. Apparently, these connections with mixed angle screws are suitable for seismic design of CLT buildings with moderate or high ductility in New Zealand.

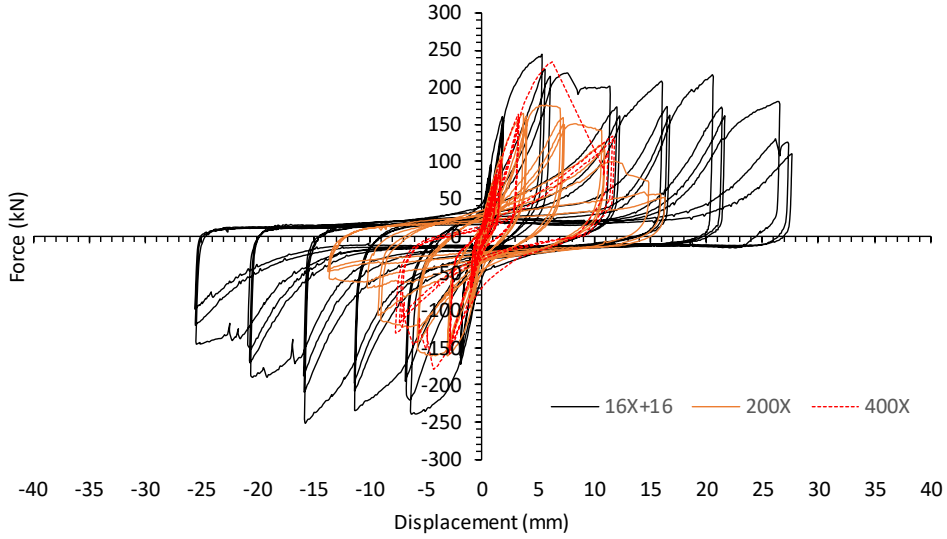

Figure 50: CLT5 test series

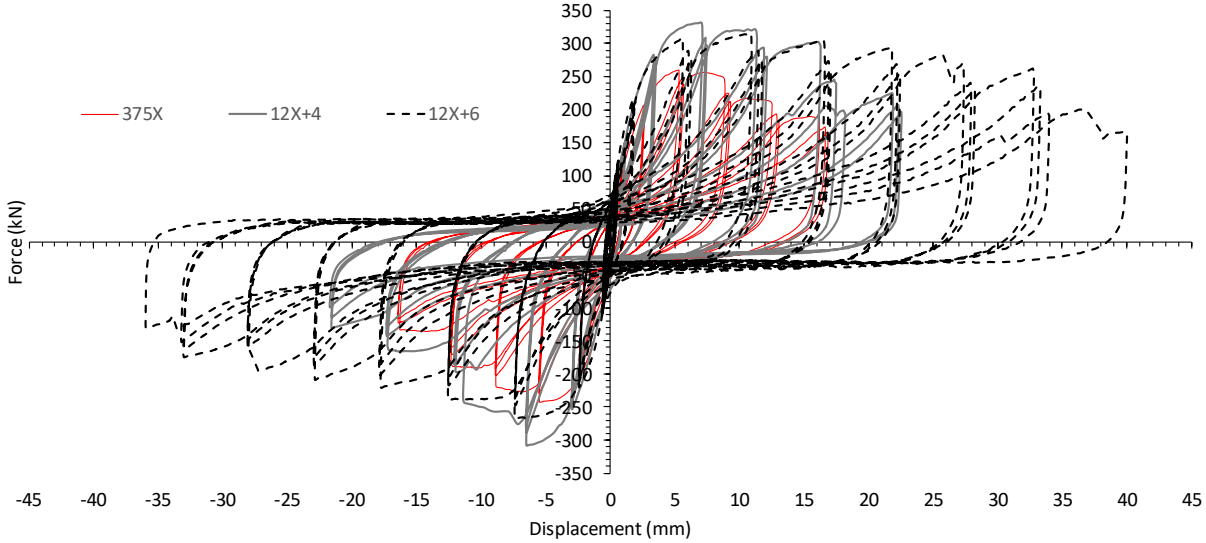

Figure 51: CLT7 test series

By controlling the screw embedment length, tensile failure of the screws could be minimized. For the connections with mixed angle screws, the timber embedment crushing was noticeably larger. This is consistent with the increased displacement capacity shown in Figure 50 and Figure 51.

Figure 52: Screw install

Figure 55: CLT5-8T test - 80mm displacement

Figure 53: CLT7-375X - Screws post test

Figure 56: CLT7-375X - Timber embedment crushing

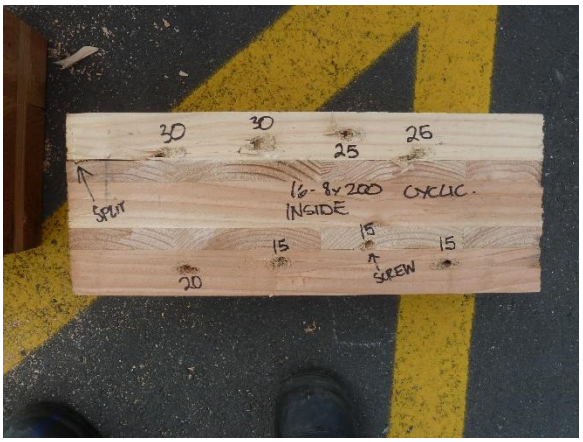

Figure 54: CLT5-200X - Timber embedment crushing

Figure 57: CLT5-16X+16 - Timber embedment crushing

5.2 Castellated Connection Testing

Figure 58 and Figure 59 show the strength predictions and the experimental test results of the castellated connections in CLT5 and CLT7 loaded perpendicular and parallel to grain of the outer CLT layer, respectively. Apparently, further work is required to better understand the load transfer in the connections loaded perpendicular to grain of the outer CLT layer. However, the analytical predictions for the connections loaded parallel to grain of the outer CLT layer agreed reasonably well with the test results.
The experimental results showed the great benefit of CLT having cross-layer reinforcement to prevent sudden brittle failure in wood. Figure 59 shows that after longitudinal shear failure of the outer CLT layers, which is typically a brittle failure, the connections were still able to sustain the load as the cross layers were still engaged to transfer the load in compression perpendicular to grain.

5.2.1 Load perpendicular to grain of outer CLT layer

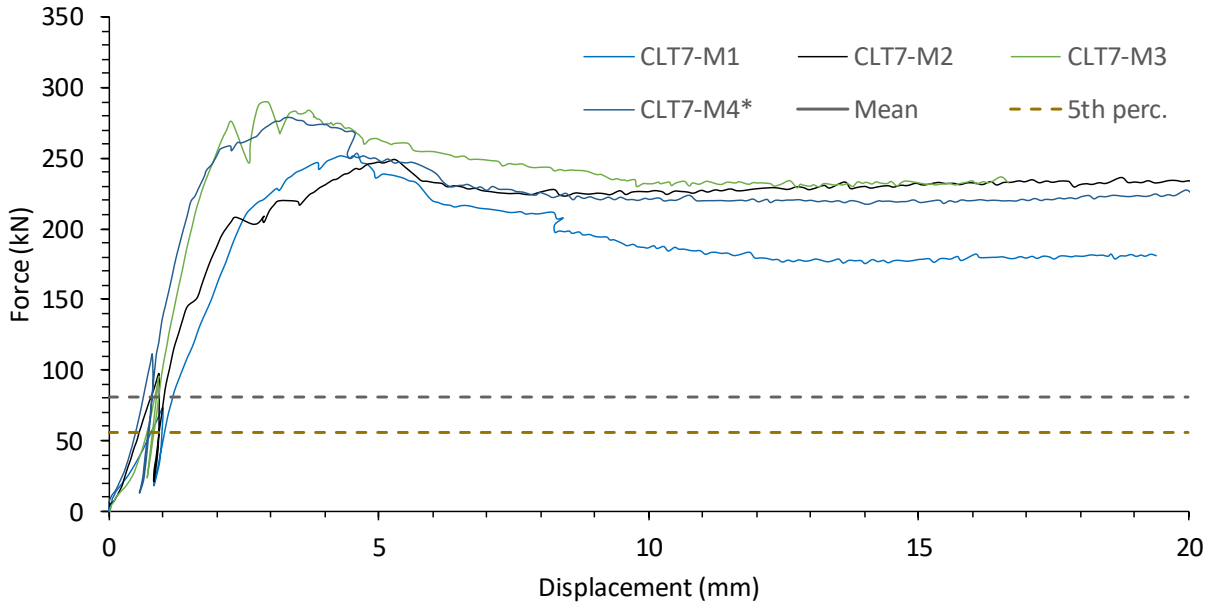

Figure 58: C2 test series comparison to analytical prediction

5.2.2 Load parallel to grain of outer CLT layer

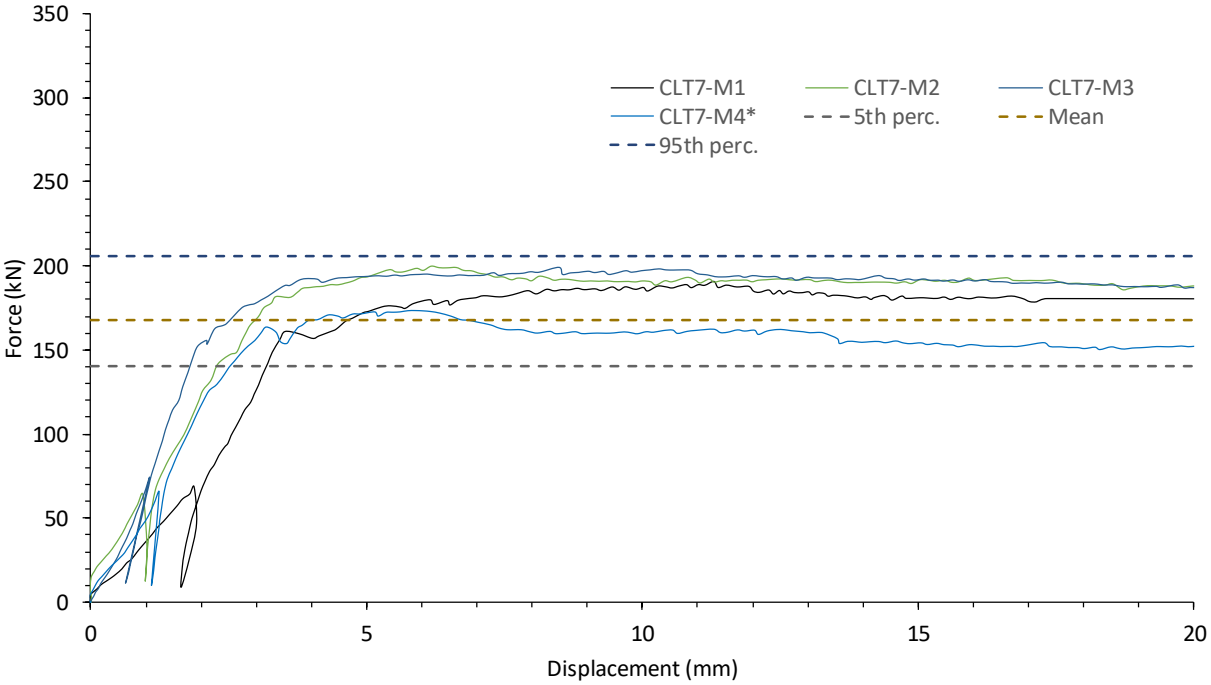

Figure 59: C4 test series comparison to analytical prediction

Figure 60: CLT5 - C1 test series

Figure 61: CLT5 - C3 test series

Figure 62: CLT5 - C1 test series

Figure 63: CLT5 - C3 test series

5.3 Core-wall System Testing

5.3.1 Phase I – Single wall testing

The single wall testing was designed so that its test results can be used to calibrate a core-wall prediction model in future development. Preliminary results and the predictions are shown below.

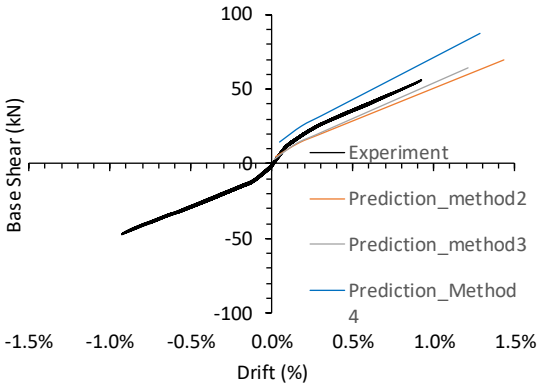

Figure 64: Force-displacement

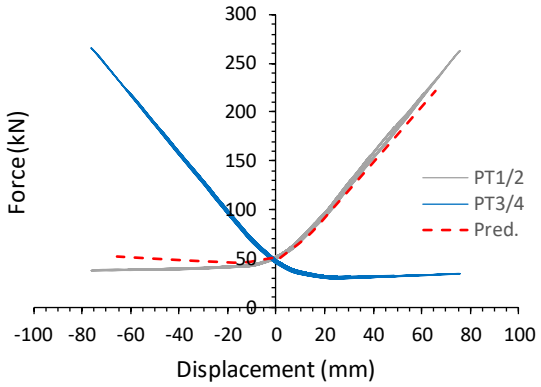

Figure 65: post-tensioning force-displacement

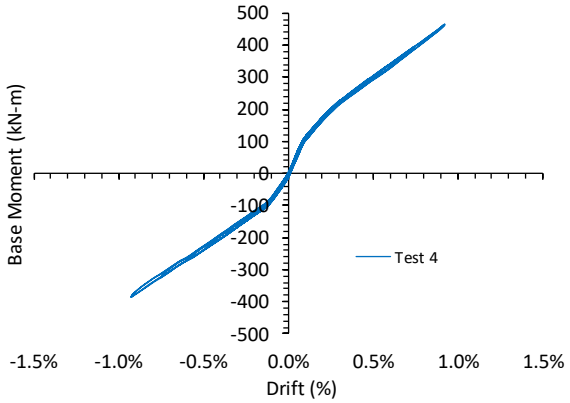

Figure 66: Moment-drift

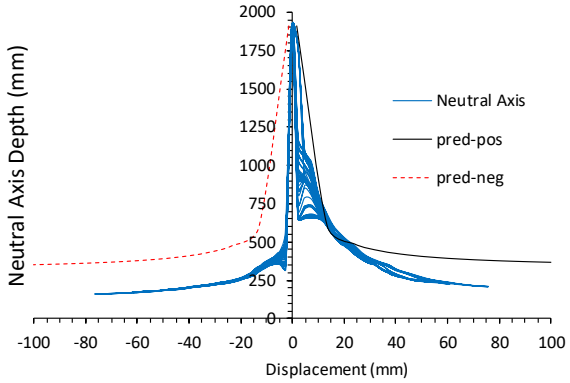

Figure 67: Neutral axis depth-displacement

Prediction of location of the neutral axis, which is a function of the post-tensioning force, is critical to an accurate analytical model. Figure 65 shows that the strain of the timber compression zone and the decrease in post-tensioning force need to be further refined.

In order to better understand the compression zone of rocking interface, see Figure 28, particle tracking velocimetry (PTV) has been used throughout the test programme. Streams 3.00 (Nokes, 2017) is an image processing and PTV system designed and implemented at the University of Canterbury in the field of fluid mechanics. By using PTV in this testing, we aimed to capture the shifting of neutral axis of the post-tensioned system under lateral loads. Figure 68 below shows the experimental set-up where 10 digital cameras were placed around the base of the specimen to capture and track the movement of dots attached on the CLT wall.

Figure 68: PTV set-up with cameras and lighting

5.3.2 Phase II – Coupled wall testing

In the coupled wall testing, increased strength and stiffness was observed when the density of screws between the walls increased. No brittle failure was observed throughout the tests; however, the specimen was not pushed to large drift ratios to avoid too much damage in the CLT panels. Figure 69 shows the movement of the base of the coupled wall. Gap opening at the base interface can be observed. In general, local embedment crushing in plywood splices and CLT panels was observed at the in-plane joint.

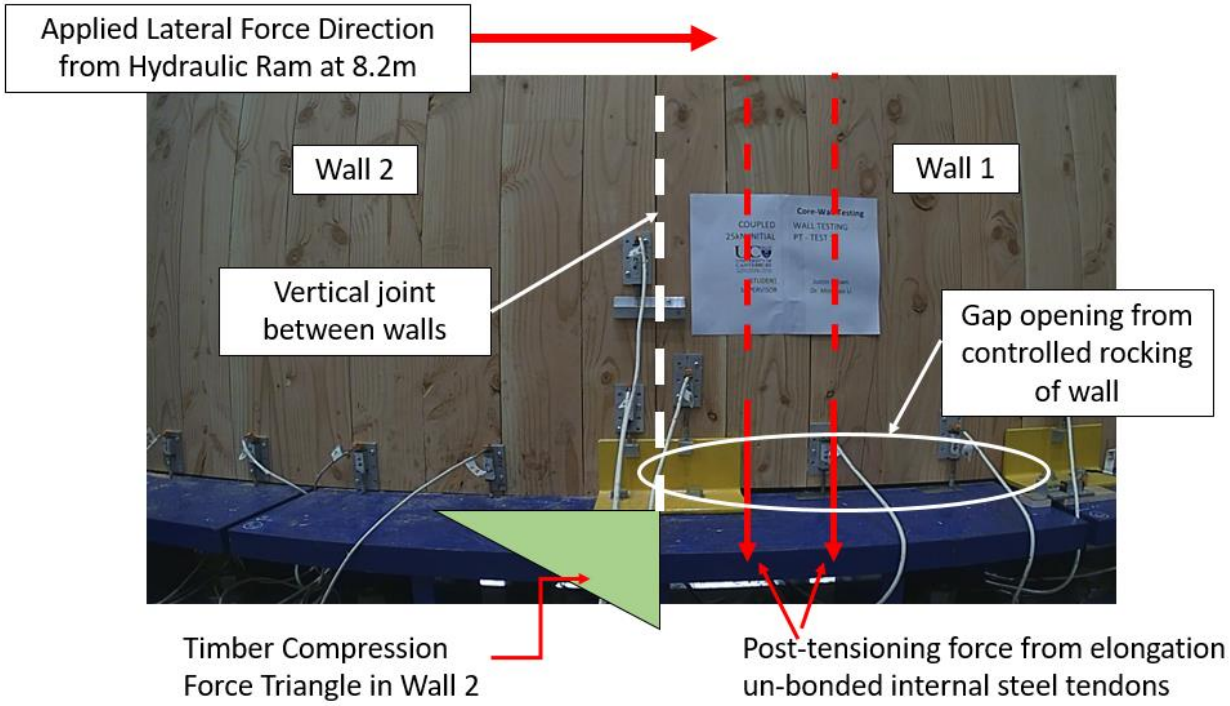

Figure 69: Coupled wall base interface

The in-plane connections between the wall panels used plywood with screws installed at 90 degrees. These connections were not able to provide a very stiff connection system. Nevertheless, they provided a cost effective connection solution that can achieve a certain level of composite action in the coupled wall. Figure 70 and Figure 71 show the significant wood embedment crushing in the screwed connections, indicating a ductile failure mode of these connections.

.

Figure 70: Plywood crushing

Figure 71: CLT crushing / embedment

U-shaped flexural plates (UFPs) were also installed at the base of the walls to provide additional energy dissipation. The inclined screwed connection detail to the CLT wall worked well in provided a strong and stiff connection such that the UFPs could yield, as shown in Figure 72.

Figure 72: Yielding of UFP

5.3.3 Phase III – Core-wall testing

5.3.3.1 Post-tensioned core-wall

Increased composite action was observed during core-wall testing when stiffer connections with inclined screws between the wall panels were used. However, as shown in Test 5, in addition to increased stiffness displacement capacity of the connections is critical and sudden loss of stiffness due to brittle failure of the connections should be avoided. In this regard, strong, stiff, and ductile connections were installed on both the orthogonal joints and the in-plane joints in Test

6. In Test 6, a peak force of 845 kN was reached at 2.3% drift of the wall. Figure 73 and Figure 74 show the slip responses of the orthogonal joints and the in-plane joints with respect to the displacement at the top of the wall.

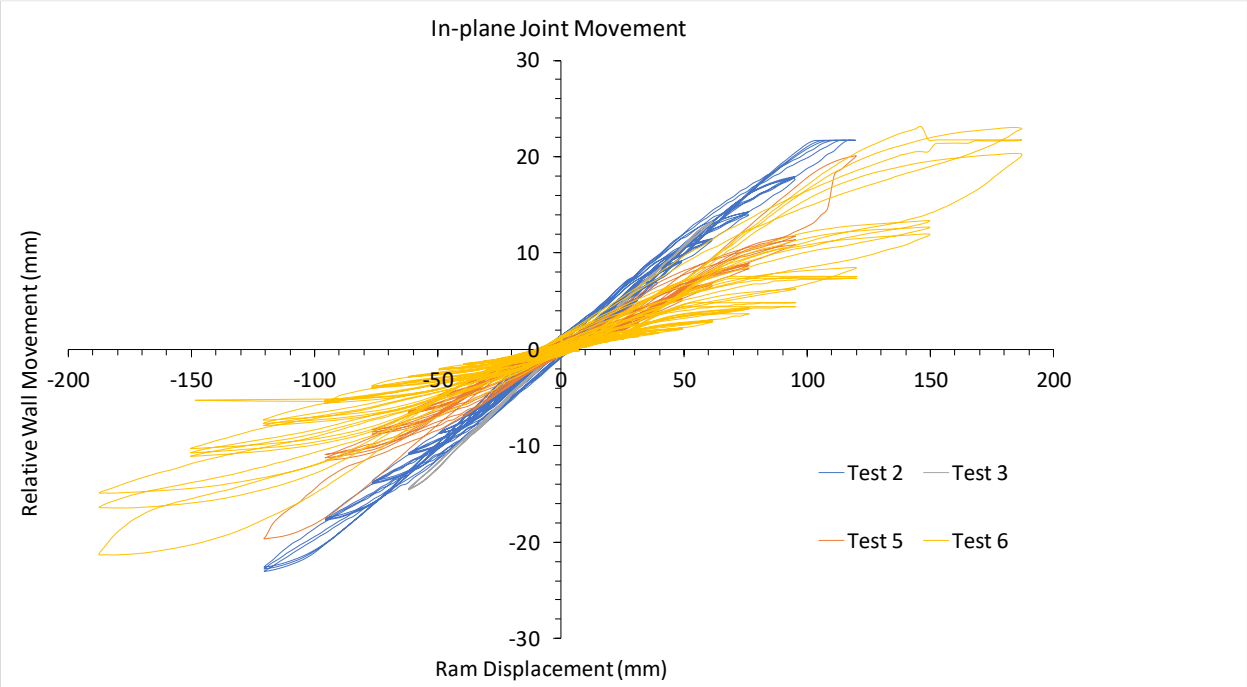

Figure 73: In-plane joint movement

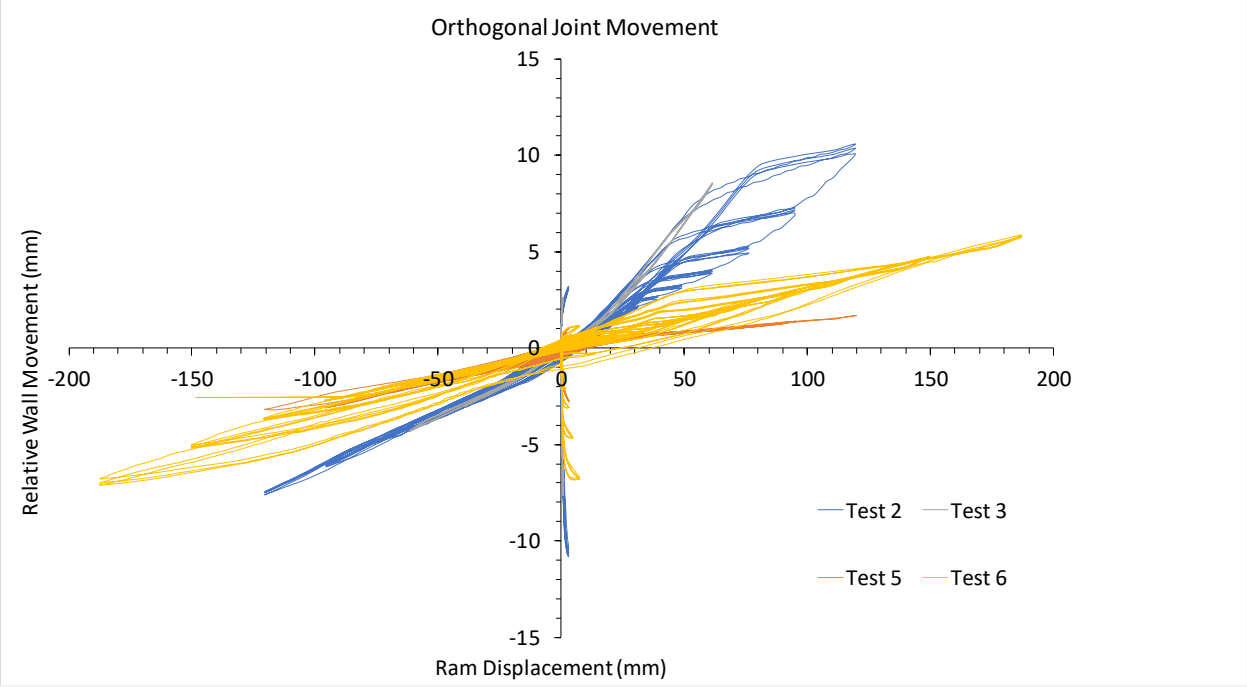

Figure 74: Orthogonal joint movement

The diaphragms were decoupled from the wall system to minimize the displacement incompatibility caused by the wall rocking mode. In this testing, diaphragms were required solely

for providing out of plane buckling restraints of the walls. To decouple the diaphragm, slotted holes were used, allowing the wall to rotate freely from the floor, as shown in Figure 75.

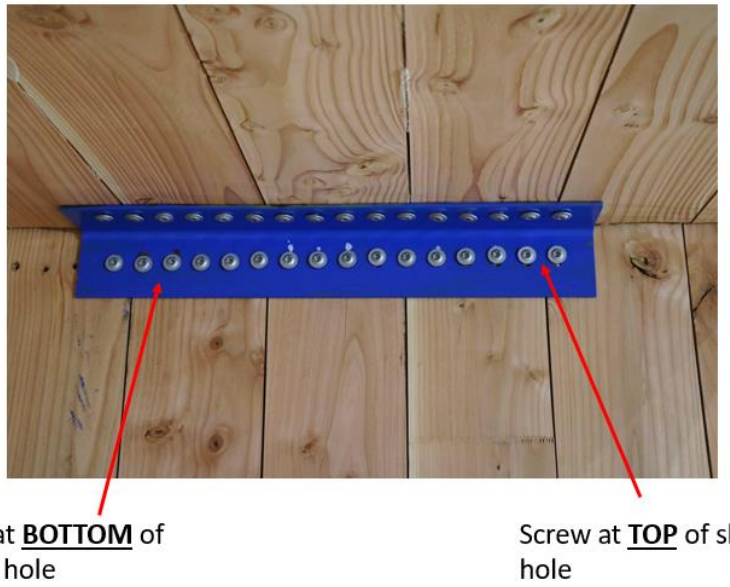

Figure 75: Diaphragm-wall connection detailing

Figures 76~81 show the photos of various types of screwed connections used in different tests to introduce different composite actions of the core-wall systems.

Figure 76: Test 2 orthogonal joint

Figure 77: Test 2 in-plane joint

Figure 78: Test 5 in-plane joint

Figure 79: Test 5 orthogonal joint

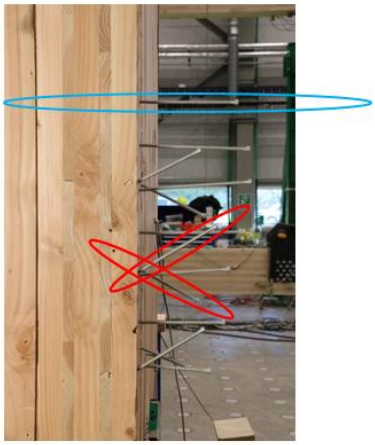

Figure 80: Test 6 orthogonal joint

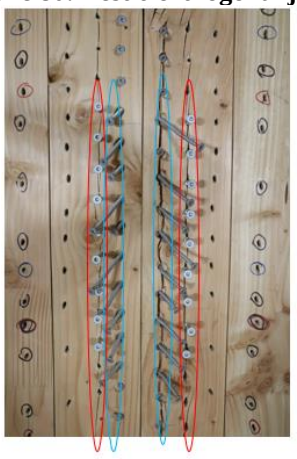

Figure 81: Test 6 in-plane joint

5.3.3.2 Conventional core-wall

In this testing, post-tensioning bars were loosened and additional hold-down connections and shear keys were installed at the base of the wall. Figure 82 show the uplifting of the base of the wall at 1.8% drift demand. In general, the hold-downs with mixed angle screws and steel side plates were able to provide significant strength, stiffness and displacement capacity. However, further study is required on this new type of hold-downs to better quantify the connection characteristics. The Titan TCN240 angle brackets were used as the shear keys at the base of the wall. A half nailing pattern was used for the Titan TCN240 brackets to ensure brittle failure mechanisms were avoided.

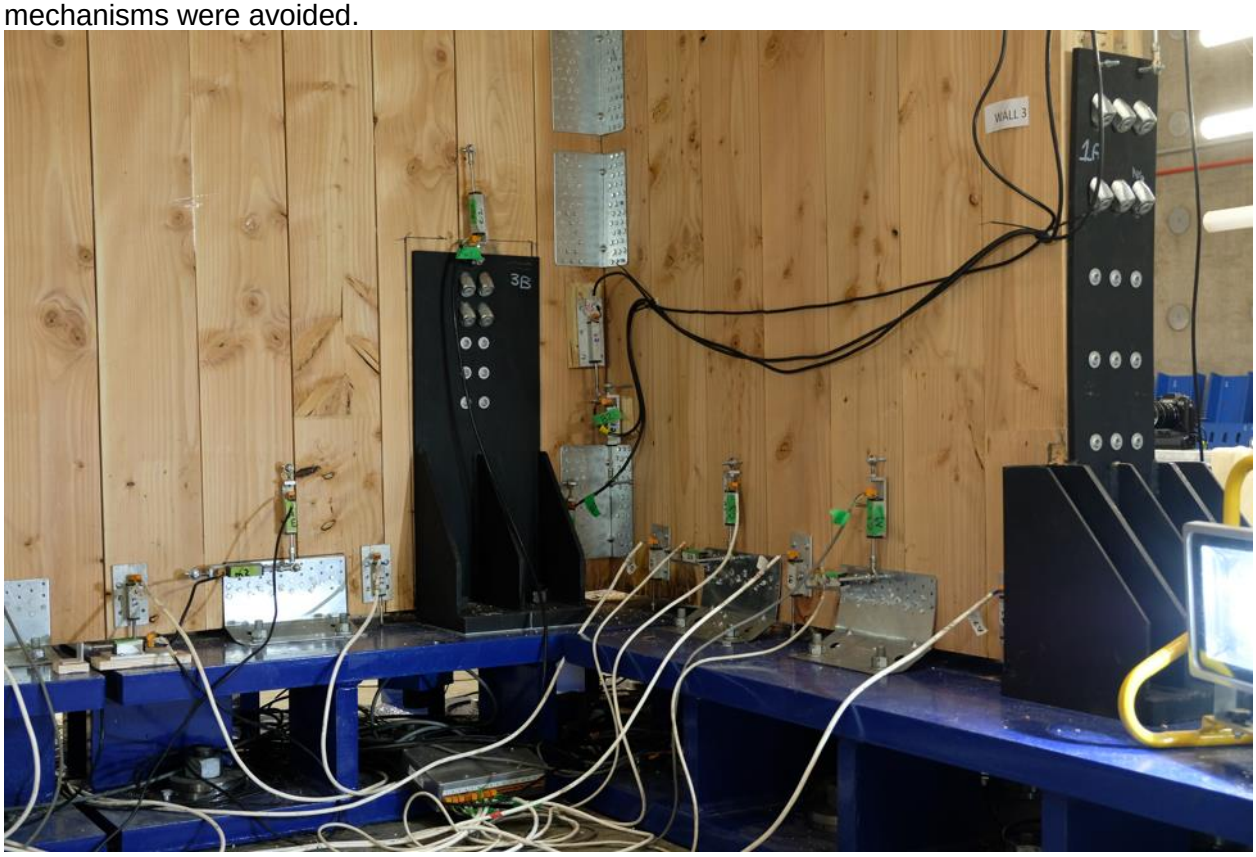

Figure 82: Test 8 at 1.8% drift

The improvement of the displacement capacity of the system is significant when compared to previous CLT -in-plane wall testing with standard nailed hold-downs. Figure 83 and Figure 84 show a comparison between Test 8 and the previous testing with CLT walls using standard nailed hold-down connectors. In Test 8, the system could sustain the peak load at increased displacements while the walls with conventional hold-downs experienced significant strength loss beyond the peak load.

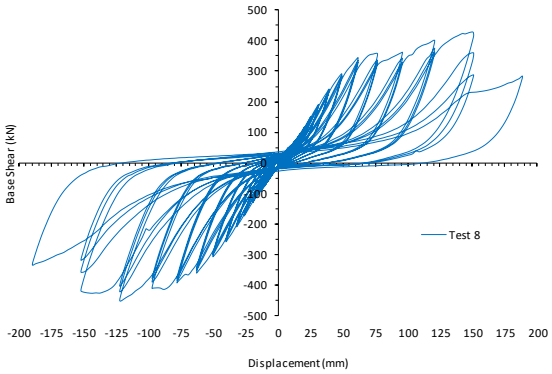

Figure 83: Test 8 force displacement curve

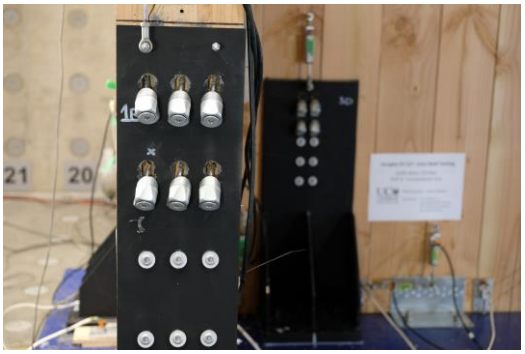

Figure 85: Inclined screw withdrawal

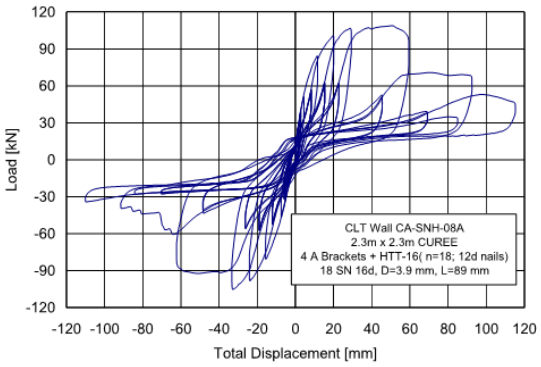

Figure 84: CLT wall with standard hold-down (Popovski, Schneider, & Schweinsteiger, 2010)

Figure 86: Nail shearing (Popovski et al., 2010)

6 ACKNOWLEDGEMENTS

The authors would like to thank University of Canterbury technicians Mr. Gavin Keats, Mr. Alan Poynter, Mr. Russell McConchie and Mr. Alan Thirwell, for their valuable input and support throughout the test programme. The authors would also like to thank University of Canterbury 3rd Pro students Mr. Dan Hydman, Mr. Ben Karalus, Mr. Chris Ravn, and Mr. Ben Scott for their work on the connection testing programme.
Additional support provided by Spax Pacific Ltd and BBR Contech Ltd. is greatly appreciated for in their respective sponsorship of screws and macalloy bars.

7 REFERENCES

ACI Innovation Task Group 5. (2008). *Acceptance criteria for special unbonded post-tensioned precast structural walls based on validation testing and commentary : an ACI standard*. Farmington Hills, Mich.: American Concrete Institute.

ASTM International. (2011). *ASTM E 2126-11: standard test methods for cyclic (reveresed) load test for shear resistance of vertical elements of the lateral force resisting systems for buildings*. West Conshohocken, PA: American Society for Testing and Materials.

Bejtka, I., & Blaß, H. J. (2002). Joints with inclined screws. *Working Commission W18 - Timber Structures, 35-7-4*, 141.

CEN. (2004). *Eurocode 5: Design of timber structures-Part 1-1: General-Common rules and rules for buildings*. Brussels, Belgium: European Committee for Standardization.

Devereux, C. P., Holden, T. J., Buchanan, A. H., & Pampanin, S. (2011). *NMIT Arts & Media Building - Damage Mitigation Using Post-tensioned Timber Walls*.

Dujic, B., Aicher, S., & Zarnic, R. (2005). Investigations on in-plane loaded wooden elements - influence of loading and boundary conditions. *Otto Graf Journal, 16*.

Dujic, B., Pucelj, J., & Zarnic, R. (2004). Testing of racking behavior of massive wooden wall panels. *Proc., 37th CIB-W18 Meeting, International Council for Building Research and Innovation*.

Dunbar, A. J. M. (2014). *Seismic design of core-wall systems for multi-storey timber buildings: a thesis submitted in partial fulfilment of the requirements for the degree of Master of Engineering in Earthquake Engineering, Department of Civil and Natural Resources Engineering, University of Canterbury . Christchurch, New Zealand*.

EN12512. (2005). *Timber structures: test methods : cyclic testing of joints made with mechanical fasteners : [including amendment A1:2005]* (English version. ed. Vol. BS EN 12512:2001.;BS EN 12512:2001;). London: British Standards Institution.

EN26891. (1991). *Timber structures - Joints made with mechanical fasteners - General principles for the determination of strength and deformation characteristics*. Brussels: British Standards Institution,.

ETA. (2012). *ETA-12-0114 - SPAX selt-tapping screws*.

Gagnon, S., Pirvu, C., & Fpinnovations. (2011). *CLT handbook: cross-laminated timber* (Canadian ed. Vol. SP-528E.;SP-528E;). Québec: FPInnovations.

Gavric, I., Fragiacomo, M., & Ceccotti, A. (2015). Cyclic Behavior of CLT Wall Systems: Experimental Tests and Analytical Prediction Models. *Journal of Structural Engineering, 141*(11), 04015034. https://doi.org/doi:10.1061/(ASCE)ST.1943-541X.0001246

Green, M., & Taggart, J. (2017). *Tall wood buildings: design, construction and performance*. Basel;Boston;: Birkhäuser.

Iqbal, A., Pampanin, S., Palermo, A., & Buchanan, A. H. (2015, Apr). Performance and Design of LVL Walls Coupled with UFP Dissipaters. *Journal of Earthquake Engineering, 19*(3), 383-409. https://doi.org/10.1080/13632469.2014.987406

Kelly, J. M., Skinner, R. I., & Heine, A. J. (1972). Mechanisms of energy absorption in special devices for use in earthquake resistant structures. *Bulletin of the New Zealand Society for Earthquake Engineering, 5*(3), 63-73.

Moroder, D. (2016). *Floor diaphragms in multi-storey timber buildings: a thesis presented for the degree of Doctor of Philosophy in Civil Engineering at the University of Canterbury, Chrictchurch, New Zealand*.

Newcombe, M. P. (2011). *Seismic Design of Post-Tensioned Timber Frame and Wall Buildings*).

Nokes, R. (2017). *Streams: System Theory and Design*.

Palermo, A., Pampanin, S., Buchanan, A., & Newcombe, M. (2005, 2005). *Seismic design of multi-storey buildings using laminated veneer lumber (LVL)*.

Palermo, A., Pampanin, S., & Buchanan, A. H. (2006, 2006). *Experimental investigations on LVL seismic resistant wall and frame subassemblies*.

Palermo, A., Pampanin, S., Fragiacomo, M., Buchanan, A. H., & Deam, B. L. (2006, 2006). *Innovative seismic solutions for multi-storey LVL timber buildings*.

Pampanin, S. (2005). Emerging Solutions for High Seismic Performance of Precast/Prestressed Concrete Buildings. *Journal of Advanced Concrete Technology, 3*(2), 207-223. https://doi.org/10.3151/jact.3.207

Pampanin, S., Palermo, A., & Buchanan, A. (2013). *Post-Tensioned Timber Buildings - Design Guide Australia and New Zealand*: Structural Timber Innovation Company.

Piazza, M., Polastri, A., & Tomasi, R. (2011). Ductility of timber joints under static and cyclic loads. *Proceedings of the Institution of Civil Engineers: Structures and Buildings, 164*(2), 79-90. https://doi.org/10.1680/stbu.10.00017

Popovski, M., Schneider, J., & Schweinsteiger, M. (2010). *Lateral load resistance of cross-laminated wood panels.* Paper presented at the 11th World Conference on Timber Engineering 2010, WCTE 2010.

Priestley, M. J. N. (1991). Overview of PRESSS research program. *PCI JOURNAL, 36*(4), 50-57.

Sarti, F. (2015). *Seismic design of low-damage post-tensioned timber wall systems: a thesis submitted in partial fulfilment of the requirements for the degree of Doctor of Philosophy in Civil Engineering at the University of Canterbury, Christchurch, New Zealand*.

Seagate Structures. (n/a). UBC Brock Commons. Retrieved from https://seagatestructures.com/projects/brock-commons/

Smith, T. (2014). *Post-tensioned timber frames with supplemental damping devices: a thesis presented for the degree of Doctor of Philosophy in Civil Engineering at the University of Canterbury, Christchurch, New Zealand*.

Tomasi, R., Crosatti, A., & Piazza, M. (2010). Theoretical and experimental analysis of timber-to-timber joints connected with inclined screws. *Construction and Building Materials, 24*(9), 1560-1571. https://doi.org/https://doi.org/10.1016/j.conbuildmat.2010.03.007

Tomasi, R., Piazza, M., Angeli, A., & Mores, M. (2006). A new ductile approach design of joints assembled with screw connectors. *Proceedings of 9th World Conference on Timber Engineering, Portland, OR.*